RAPID DIGITIZATION AND NON-RIGID REGISTRATION OF AEROSPACE BLADE GEOMETRIES FOR HYBRID MANUFACTURING COMPONENT REPAIR

A Dissertation
Presented to
The Academic Faculty

by

Myong Joon Kim

In Partial Fulfillment
of the Requirements for the Degree
Master of Science in the
School of Mechanical Engineering

Georgia Institute of Technology
May 2019

RAPID DIGITIZATION AND NON-RIGID REGISTRATION OF AEROSPACE BLADE GEOMETRIES FOR HYBRID MANUFACTURING COMPONENT REPAIR

Approved by:

Dr. Christopher Saldana, Advisor
School of Mechanical Engineering
Georgia Institute of Technology

Dr. Thomas Kurfess
School of Mechanical Engineering
Georgia Institute of Technology

Dr. Shreyes Melkote
School of Mechanical Engineering
Georgia Institute of Technology

Date Approved: December 13, 2018

ACKNOWLEDGEMENTS

First, I would like to sincerely thank Dr. Christopher Saldana for his guidance, insight, and support as an advisor. I would like to thank him for providing me an opportunity to participate in a project and conduct research. I would also like to thank Dr. Kurfess and Dr. Melkote for their time and commitment to be on my committee. I would also like to thank Delta Airlines for their funding and the project, and Mr. Raymond Romesburg for his industrial knowledge and advice. I would like to thank Maxwell Praniewicz for his knowledge in machining and software, and his help as a research colleague. I would like to thank Steven Sheffield and Nathan Mauldin for their advice in machining. I would like to thank the past and the current students in Dr. Saldana's lab for help with their support. I would like to thank the students and faculty of the PMRC for help with their support. I would like to express my genuine gratitude to my family for their endless trust and support; without you all, I would not be here.

TABLE OF CONTENTS

LIST OF TABLES

LIST OF FIGURES

LIST OF SYMBOLS AND ABBREVIATIONS

Zn	horizontal 2D blade profile
N	number of 2D profiles along the entire blade
Nnom_zi	2D profiles on nominal blade
Ndef_zj	2D profiles on deformed blade
W	number of profiles in the weld height
S	number of segments in 2D profile
P	number of points in one segment of 2D profile
H	order of fitted polynomial on thickness distribution

SUMMARY

Using hybrid manufacturing strategies provides an opportunity to automate the entire process of repairing airfoil components, which involves processes that include preparing for pre-weld airfoil, wire-feed welding, on-machine probing, blending, and polishing. To achieve the above requires both rapid digitization and non-rigid registration methods to fully utilize additive and subtractive manufacturing process to achieve high dimensional accuracy, time and material efficiency. In this study, several profile digitization strategies are investigated to determine effects on accuracy of the final non-rigid registration of the component geometry and the impact on the quality measures pertaining to parent material blendlines. These profile digitization strategies include approaches based on curvature-based segmentation, G1 and G2 continuity, and local control of maximum profile deviation. From these results, it was seen that by locally controlling maximum profile deviation, it is possible to achieve acceptable profile tolerance limits while limiting the number of points required for profile digitization.

.

INTRODUCTION

1.1 Motivation and problem statement

Repair, or remanufacture, of jet engine components to extend the life cycle of aerospace parts has been a great interest to aerospace industries due to the high overhaul cost, high cost of new condition parts, and the inefficient process of recycling partially worn parts [1]. Approximately 8% of the operating costs of an airplane are due to jet engine maintenance, and 50% of the overhaul costs are due to the airfoils [2]. Moreover, the complex geometry of the components and required unique alteration of each part due to part-specific deformations requires continuous intensive work, multiple setups between different stations, and skill intensive manual operations including additive manufacturing (AM), subtractive manufacturing (SM), and sanding to name a few. Inconsistency in worker skill level in production is detrimental to strict quality assurance and contributes to overall ineffectiveness in time and cost as well as inconsistency of the final product. This leads to high scrap rate and operating cost in the overhaul [3,4].

An attractive solution to curtail the inconsistency in the blade repair process and implement fully automated strategies is to combine all procedures on a flexible processing platform, which is referred to as hybrid manufacturing (HM). When used blades are determined to be serviceable, HM strategies are capable of interchanging between subtractive and additive manufacturing to repair standard blades without major post processing and manual operations. Each operation is well established, but the individual repair currently relies on manual, semi-automated welding, blending, grinding, and polishing. HM strategies integrating all processes have not been made widely available in

the commercial airfoil repair market [5,6]. The absence of a complete integration of the HM solution provides for a significant opportunity for research in this area to eliminate inconsistency and inefficiency in this process and further achieve advanced productivity and quality assurance [7]. This would have the added benefit of reducing the scrap rate.

One commercially available HM strategy, RECLAIM (Remanufacture of high value products using a Combined Laser cladding, Inspection and Machining system) [1], has previously been developed and introduced, however, the associated probing strategy and the reconstruction of the remanufactured region present several limitations. The RECLAIM process claims to provide for adaptive integrated SM and AM strategies to remanufacture aerospace turbine blades. This paper introduces processes involving probing, welding, and blending of the blade tip with the ability to cope with "the extreme variation in volume, product mix, and product condition" [2]. The paper presents promising results in adaptive re-tipping of the blade with less than 0.0004 inch of mismatch between parent material and the blended region as well as good fusion of the weld on the parent material. However, the paper presents some methodological limitations: (1) a probing and morphing algorithm was not applied to the additive welding process for adaptive path planning, (2) the probing and morphing algorithm was not explicitly explained, (3) limited quantitative analysis was provided regarding the consistency of repaired blade profiles.

An adaptive geometry transformation proposed in Ref. [8] involved a morphing algorithm to non-rigidly register the golden (or ideal) blade geometry to the deformed blade geometry to accurately interpolate the tip geometry underneath the weld, which accounts for angular distortion, lean, and wear of the blade and inconsistency in fixturing. Morphing a serviceable blade is necessary in the adaptive hybrid repair manufacturing of the blade

geometry because each blade exhibits unique deformation after the service and the accuracy of registration determines the final repaired product. However, optimization of probing and reconstructing strategies of cross sectional profiles of the parent material was not discussed in Ref. [8], this is the focus of the present study.

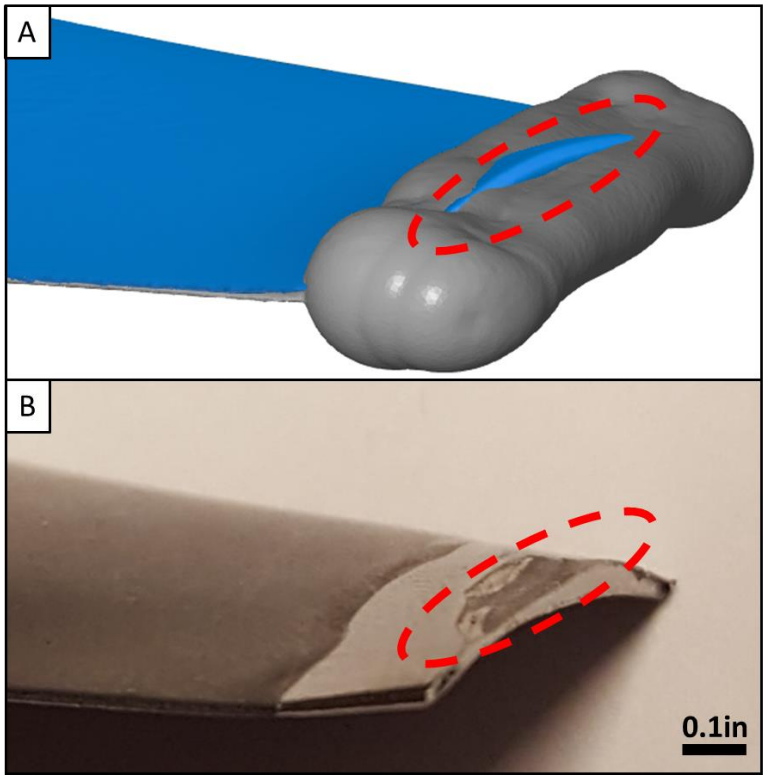

Figure 1 (A) Structured light scan of pre-welded blade (blue) and post-welded blade (grey). Not enough weld is deposited on convex side of the blade (red dashed oval); (B) The weld is machined, and the tip geometry is revealed to leave defected region (red oval).

1.2 Proposed approach

The overall approach for rapid digitization and non-rigid registration of the blade geometry is shown as a flowchart in Figure 2. This study proposes an optimized probing strategy to implement in a hybrid manufacturing process to recreate 2D profiles which are then utilized to construct unknown 3D geometry of a surrogate blade. The final inspection

was done on the blendline region of the registered nominal blade compared against that of the deformed blade to characterize surface deviation and step size. In the additive process, the registered 3D tip geometry guides an adaptive additive toolpath to not only increase material efficiency [8], but also to prevent the problem of potentially having insufficient weld material to carry out the repair (Fig. 1b). Once the tip is welded, a subtractive toolpath is created on the registered blade which will machine the weld to the repaired tip geometry without having a step between parent material and the blended region. The registered blade and deformed blade were quantified in various simulation software and were also CNC machined and inspected optically and using a coordinate measurement machine (CMM).

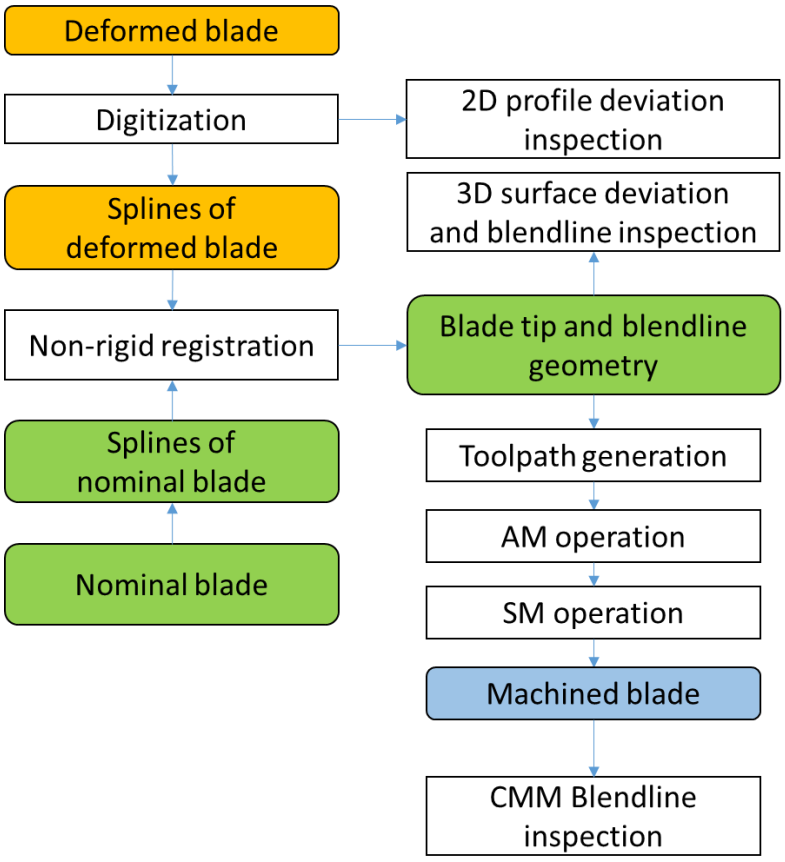

Figure 2 Overall strategy of digitization of the deformed blade and registration of the nominal blade for blending operation and inspection.

1.3 Thesis organization

The remainder of the thesis is organized as follows. Chapter 2 presents a literature review of the current state of the repair processes and the challenges in aerospace engineering, geometric digitization/registration methods, and an exploration of developed methods for adaptive repair processes. Chapter 3 mainly introduces a detailed description of novel profile digitization and reconstruction methods on a surrogate blade geometry, and the implementation of the digitization methods to non-rigid registration algorithm. Chapter 4 presents the outcome of 2D profile and 3D surface deviation resulted from proposed digitization methods, and the comparison between simulated and measured results from machined blades. Chapter 5 discusses the original contributions of the study and recommendations for the future research.

LITERATURE REVIEW

This chapter reviews past research presented in the literature. The chapter covers the following research areas and methods suggested in numerous patents: 1) repair of jet engine components in aerospace industry, 2) challenges in airfoil repair processing, 3) registration of deformed blades, and 4) adaptive repair solutions using various digitization methods.

1.4 Repair processes and methodologies in aerospace industry

As the aviation sector has been increasing its revenue for passenger and cargo operations at a consistent rate of 4-5% a year, the servicing of commercial engines involving maintenance, repair and overhaul (MRO) is also growing in need [9]. In terms of aeroengines, Rolls-Royce predicts approximately 68,000 aircraft deliveries over the period of 2012-31, with a $975 billion market value [10]. GE Aviation claims that the service market for 2011 was 46% higher than the new engine market which was $4.9 billion [11]. This necessitates growing market in the development and introduction of advanced technology in MRO repair sectors.

Commercial aircraft maintenance, repair, and overhaul (MRO) is a fundamental prerequisite to guarantee that aircraft are maintained in pre-determined states of airworthiness in safely transporting travelers and cargo. There are over 70 companies worldwide that are involved in MRO such as heavy airframe maintenance, components maintenance, engine overhaul, and line maintenance. Especially, the repair of worn or damaged components is of large interest for aerospace industries to lengthen the

component life cycle [12]. Structural and component maintenance are critical in maintenance programs which have evolved for decades as new types, materials, and technologies are applied to aircraft structures and engines [13]. Most of the weld-blend repairs are conducted on airfoil tips, nozzle guide vanes, and shroud seal fins [14].

1.5 Challenges in airfoil repair process

The repair of jet engines is of main interest for airline operators because the costs associated with these systems are primarily produced by the replacement of used blades from the high-pressure turbine [2]. These blades are costly to purchase and experience significant thermomechanical loads in operation, so commercial airline repair companies aim to save as many of the worn blades that satisfiy the required functional properties. The methods of repairing airfoils have been developed and the existing methods are keep improving to increase process efficiency in methodologies in and to lower the cost of MRO [15].

One of the challenges faced in remanufacture of aerospace components is that of the required material properties. High pressure compressor blades are core functional components which are required to be made resistant to high temperature and pressure through wear-resistant materials. Single crystal titanium-based and nickel-based alloys have been improved with various manufacturing techniques and new alloy compositions that have excellent resistance to creep and strength properties for enduring harsh service conditions, as shown in Figure 3 [16]. These materials, on the other hand, are also challenging for conventional machining processes due to high cutting forces, high tooling costs, and long machining times, which inevitably results in lower process efficiency [15].

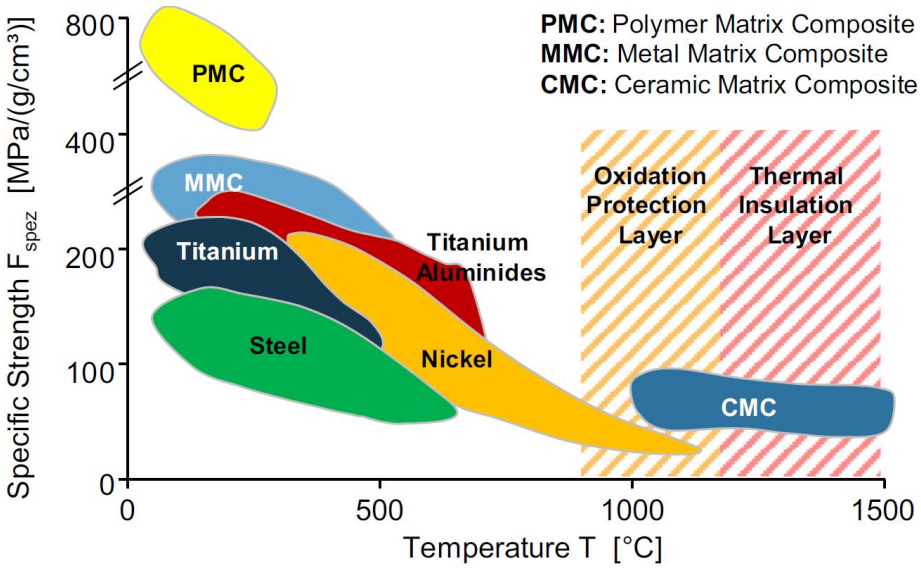

Figure 3 Specific strength (F_{spez}) of materials defined by working temperature resistance [17,18].

The other common challenge in remanufacturing the airfoil blade tip lies in the complex aerodynamics and 3D geometry of the blade that is crucial for the fuel efficiency and performance of jet engine [19]. Special geometries designed for aerodynamic and thermodynamic advantages are used in the airfoil cross-section, and involve control of twist and part angles along the stacking axis of the blade geometry [20]. During the service life of the airfoil blades, the blades suffer wear, distortion, and crack from the high rotational speeds, high pressure and high temperature. These effects can contribute to presence of foreign object debris in terms of hard particles, cause thermal expansion or contraction, cause thermal fatigue, and/or cause unwanted material contact with oxidizing or corrosive gases [21]. Further, the deformation and wear of each blade is also unique even when compared to similar blades in the same compression stage of a single jet engine [22].

Initial airfoil repair procedures were carried out in a predominantly manual fashion because they involved multiple processes ranging from welding, blending to inspection. In

the manual repair approach, the most critical processes involve depositing the weld to the worn surface and machining the welded geometry to its original blade tip without leaving excess material or gouging the parent material. Manual operations for achieving this goal require high operator skill and can be cost-effective given the cost of these components [3]. However, considering the stringent quality standards associated with airfoils and their complex geometry, it is non-trivial to establish consistency in such high-skill manual processing approaches.

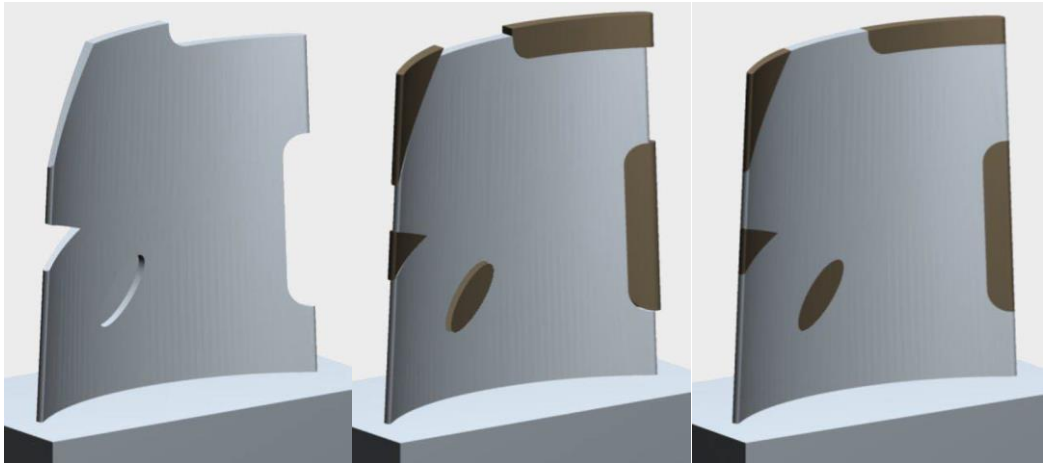

Figure 4 Standard repair procedures for the overhaul of blade geometry. (A) Weld preparation, (B) metal deposition, (C) reprofiling [23]

In summary, toolpaths are needed that can machine the weld geometry back to the nominal CAD geometry of the blade tip. However, due to the variation in the blade defects and complexity of the geometric features of an airfoil, additive and subtractive toolpaths for the deformed parts must be adaptively modified on a blade-by-blade basis. This inevitably introduces the need for accurate registration of the nominal CAD model to the deformed part that can generate adaptive toolpaths and replace manual work by automated procedures.

1.6 Registration of deformed blades

Currently, many processes in remanufacturing of blade tips are carried out manually due to reasons that can include the length of time to register the deformed parts, inaccuracy in recreating the model and creating a toolpath, and multiple setups requiring multiple registrations. An example of the proposed registration method is shown in Figure 5.

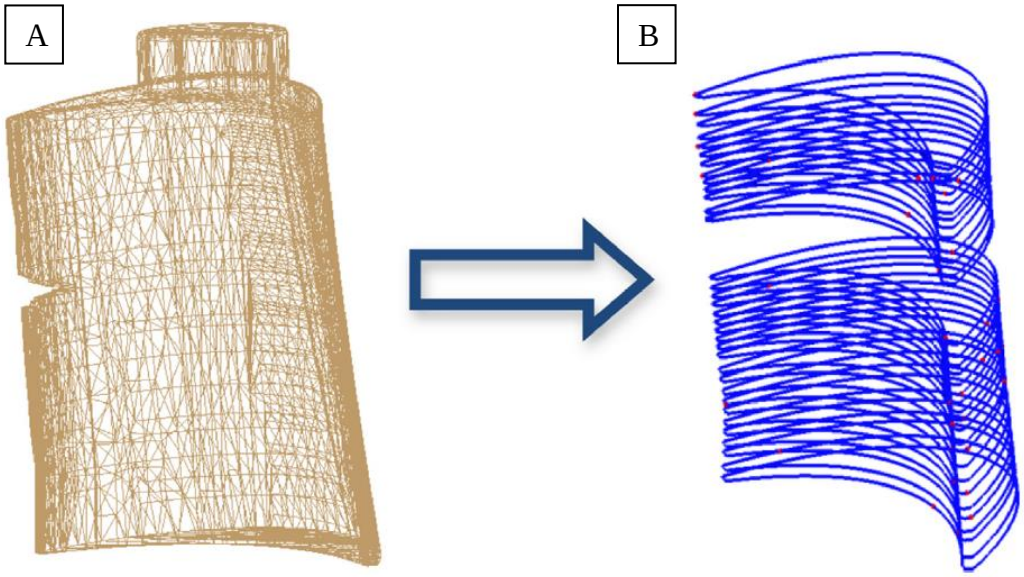

Figure 5 Proposed registration method of the damaged blade by extracting non-defective cross-sectional profiles of the blade. (A) Damaged blade mesh, (B) multiple horizontal cross-sectional surface profiles acquired [24].

The repair procedures consist of multiple steps and setups in different stations. The first step is to machine the worn tip region to expose a uniform surface for weld deposition. Next, material of the same composition as the parent material is deposited on the surface, which is then shaped using machining. Finally, abrasive post processing is applied to remove excess geometry and to achieve the surface quality standard [21]. In between each

process, appropriate inspections exist to sort out unqualified blades. Errors can occur as parts are moved and registered among multiple setups and due to the manual abrasive processing steps [25]. This provides an essential reason for implementation of registration algorithms in the automated repair process. When the registration method is involved in the automated process, the entire process can be represented as a flow chart shown in Figure 6.

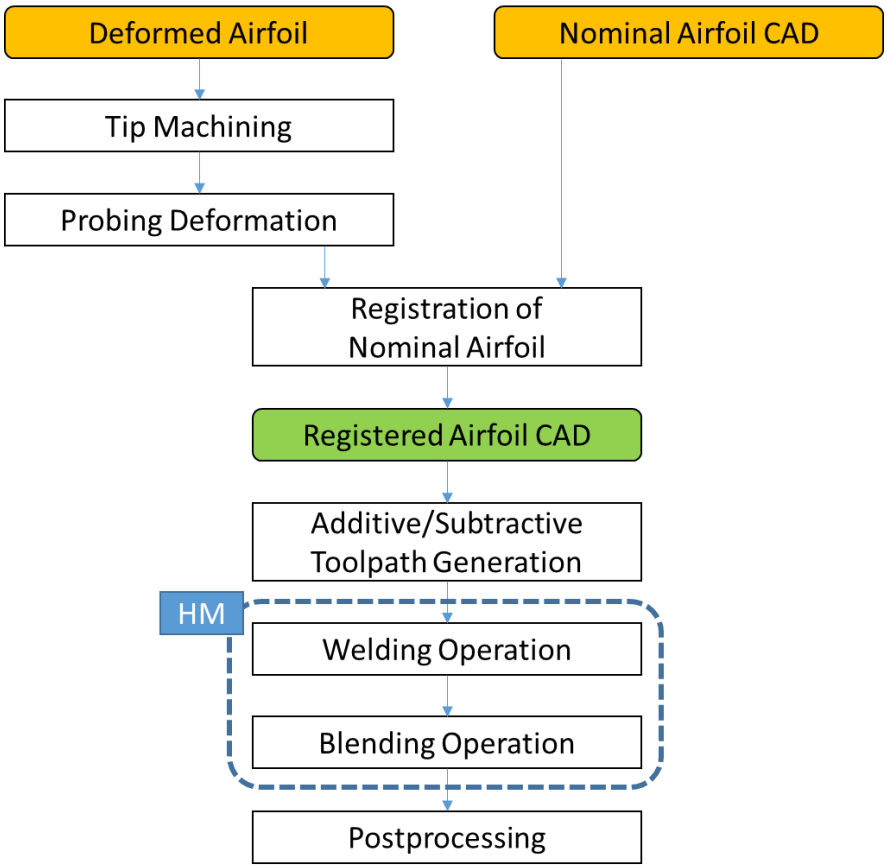

Figure 6 Automated and adaptive airfoil tip repair process encompassing registration, welding, and blending in one setting.

Registration methods have been widely studied to adapt variations in deformations of each blade in an automated repair method [3], because the quality of the final repaired product depends on the accuracy of the registered models constructed from the measured

data, the digitizing device, and the algorithm [20]. A suitable digitizing method is necessary to reconstruct deformed 3D blade model by balancing the appropriate amount of measurement information, which affects scanning time, and the accuracy of the digital reconstruction, which affects the quality of the target process plan. Quality solutions should optimize measuring time, resolution, and compatibility of the acquired data for automation [12]. Hundreds of commercially available equipment for this purpose can be categorized into three types shown in Figure 7 [26]: 1) probe contact measurement system, 2) laser scanning system, 3) topo-metric digitizing system.

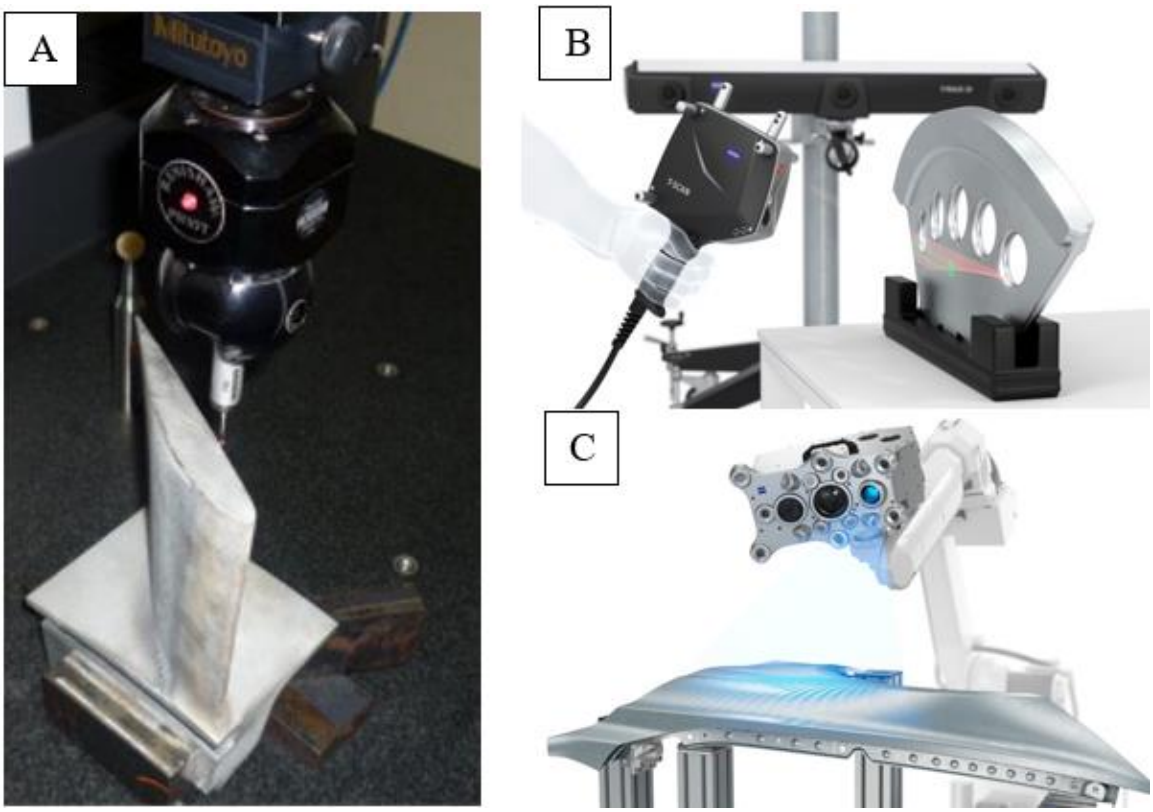

Figure 7 Three types of commercial digitizing products: (A) Renishaw probe [27], (B) Zeiss T-SCAN [28], (C) Zeiss Pro AE [29]

1.7 Adaptive repair solutions using various digitization methods

A number of studies have been made to explore digitization methods for airfoil geometries for the purpose of repair development. Walton introduced an adaptive compressor rotor tip repair solution which can refurbish the blades by digitizing the surface, constructing 3D profiles of the blade, welding and machining toolpaths generated based on the constructed geometry [12,30]. Dix developed topo-metric digitizing equipment to acquire the deformed geometry to register the nominal airfoil geometry and generated machining toolpath commands [31]. Huffman utilized a 2D vision system for controlling a laser powder fusion welding machine for blade repair [31, 32], however the 2D vision system is limited in reconstructing complex blade geometry that is based on non-linear curves. Bermer presented an adaptive machining process which digitizes two cross-sectional profiles of a straight blade under the welded volume with a probe and interpolates the tip underneath the weld [23]. Huang suggested an in-situ measurement station to digitize the contour of the component and a 6-axis finishing robot to optimize grinding and polishing process parameters [34].

While the above digitization and reconstruction algorithms and equipment have advanced capabilities in these areas, most of them are not applicable due to the lack of dimensional accuracy of reconstruction or the time required to capture the blade geometry information. In this regard, Yilmaz claims to have the most complete solution developed for an adaptive repair using a commercial software in a hybrid machine setting where it scans the deformation of the blade, welds the blade tip, and machines down with no sign of blendline steps. However, scanning time is not efficient and it never openly discussed the methods just like many other papers. Other works have investigated an adaptive

additive and subtractive manufacturing repair system, but they are not explicit about their methods and details on the results. Moreover, little work has been done that digitizes and reconstructs 2D profiles, and 3D surface geometry in simulation and validate them with actual machined measurements.

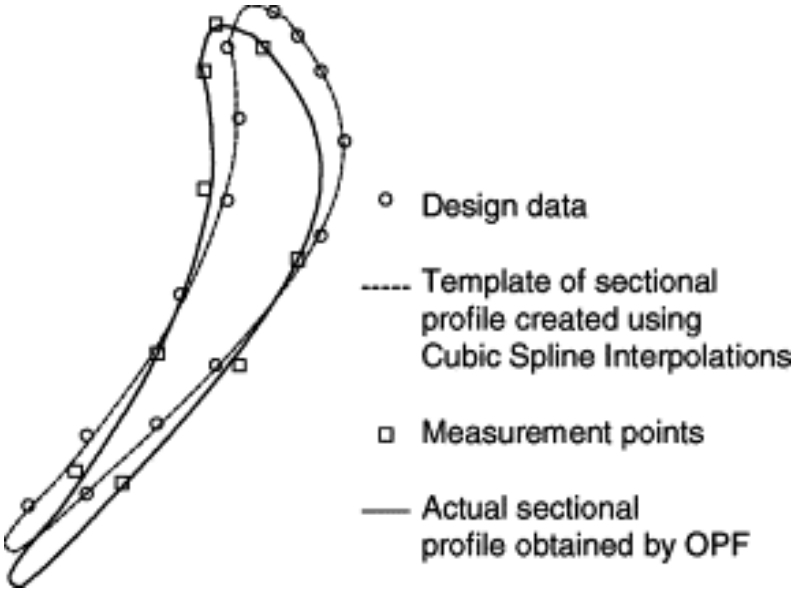

Figure 8 Comparison of two cross sections between nominal profile and actual (deformed) profile obtained by Optimal Profile Fitting (OPF) method [33], [34].

METHOD

The adaptive repair process requires integrated inspection, additive, and subtractive processing to achieve a blendline target specification for a serviced blade geometry. The entire digitization and registration strategy for an automated blending operation is depicted as a flow chart in Figure 9. In this approach, digitization of the blade geometry is needed to facilitate non-rigid registration. The target condition needed is that which achieves a sufficient target profile reconstruction specification while also limiting the number of points required, thereby reducing processing time.

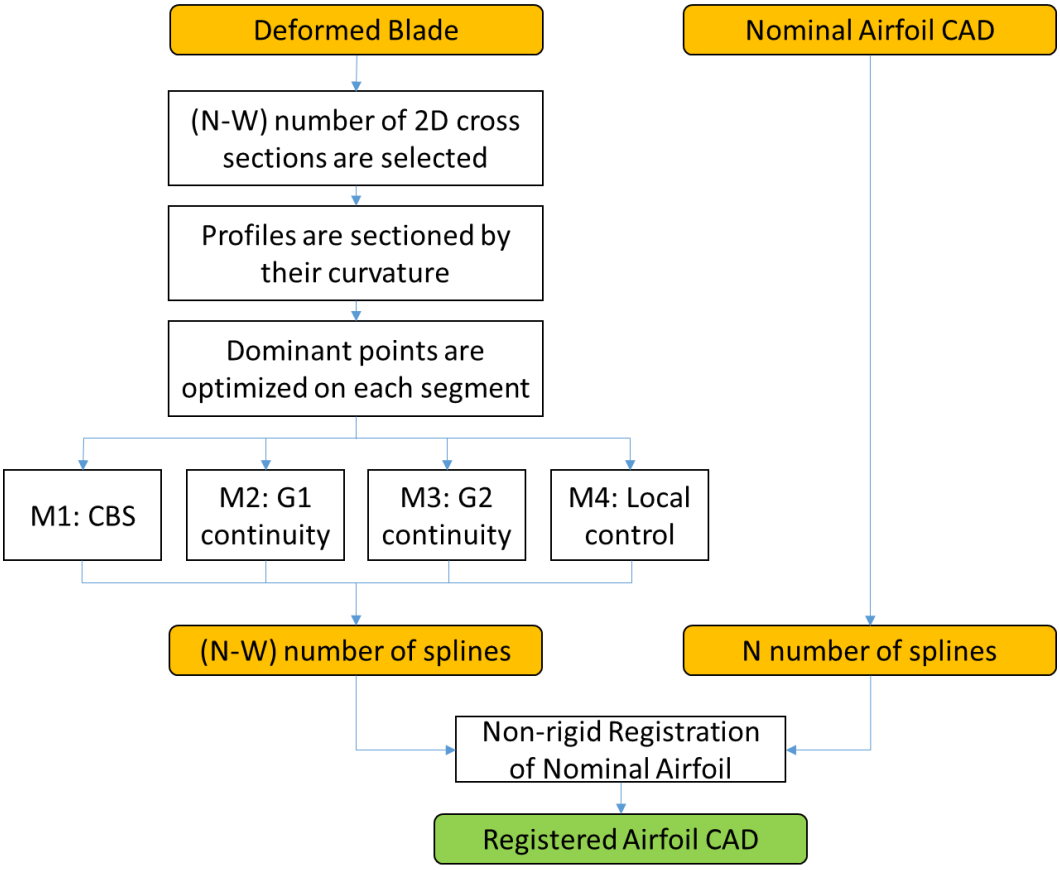

Figure 9 Overview of entire digitization and registration scheme including strategies for probing deformation with four different digitization methods.

In Figure 9, the overall goal is to produce a fully registered airfoil CAD geometry from a digitization of the deformed blade. The general geometry of airfoil models is shown in Figure 10A. The nominal airfoil CAD geometry, shown in Figure 11A, can come from the original design data or from high resolution reverse engineered scans of ideal part geometry. From this CAD geometry, a total of N cross sections perpendicular to the stacking axis (or Z axis) will be compared with that of the digitized actual blade geometry. The actual blade geometry, shown in a post-weld configuration in Figure 11B, is well understood to exhibit varying levels of deformation. In particular, angular changes and chord length changes occur along the stacking axis, as in Figure 11C, D. From this blade geometry, a total of (N-W) cross sections will be non-rigidly registered with that of the nominal CAD geometry, where W is the number of cross sections present in the weld/repair region. These W cross sections will be used to register the nominal blade to the deformed blade for interpolating the tip geometry.

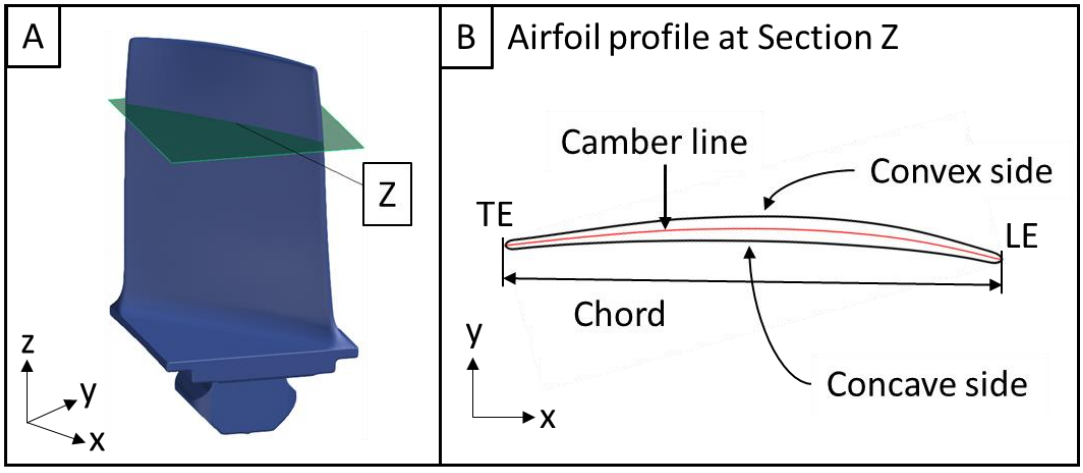

Figure 10 Basic airfoil profile. Golden model of 3D airfoil geometry and z-axis cross sectional plane (green) at the inspection height (A). Camber line, chord, leading edge (LE), trailing edge (TE), convex and concave side of the airfoil is depicted at section Z (B).

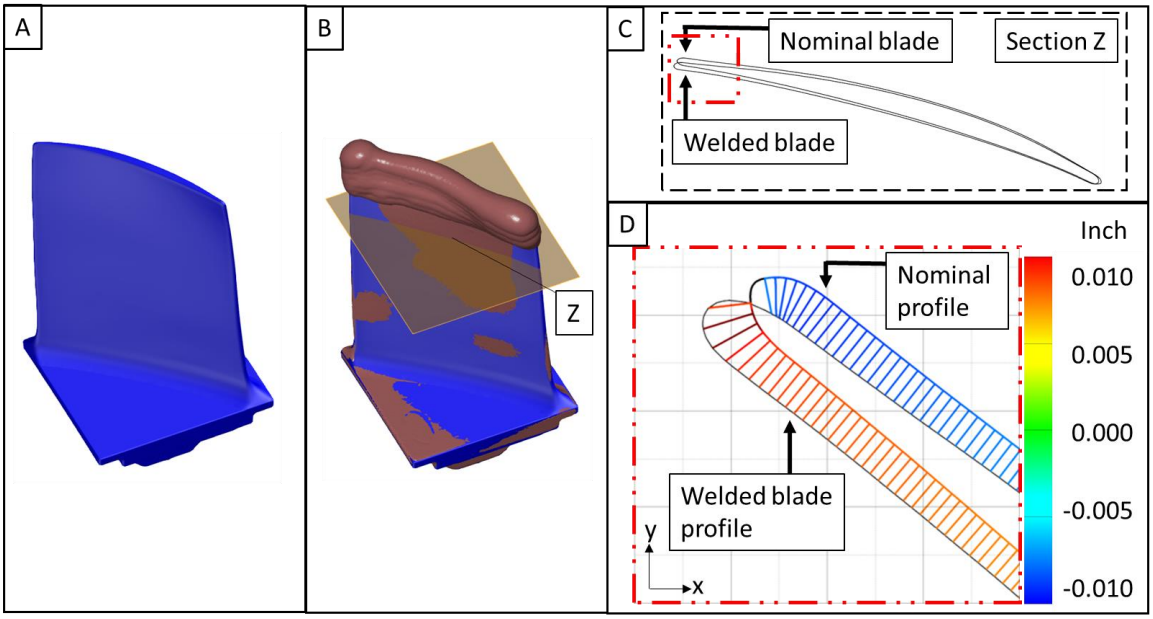

Figure 11 Images of compressor blades and cross-sectional inspection at probing height. Golden (nominal) model of a pre-weld blade geometry (A) and post-weld blade scan (grey) overlapped on the golden model (B). Cross section at Z height showing slight deviation of two models, and their deviation shown in colormap (C). Zoom-in of red dotted box (D).

1.8 Parametric design of surrogate blade

The surrogate blades are digitized in (N-W) number of 2-D cross sections below the height where the weld is present (i.e., the non-repair region), as in Figure 11B. The minimum number of dominant points on a 2-D cross-sectional profile is determined, and the points are then used to regenerate the profile with a single spline. The recreated spline should be within an acceptable tolerance from the original profile to facilitate acceptable reconstruction. In finding the minimum number of dominant points of the contour, different methods are compared in the present study, and the resulting maximum deviations, total deviations, and average deviations were used to factor out the relative differences in each method in terms of accuracy. The splines in N number of cross sections are utilized to non-

rigidly register the nominal blade and morph it to the geometry of the deformed blade. The top part of the deformed blade above the weldline (i.e., the repair region) is the final shape of the blade after the blending operation and is interpolated by the morphed nominal blade. The machining toolpath for the blending operation is derived based on the morphed nominal blade. In the present study, surface deviation and blend line height analysis are conducted between the morphed nominal blade and the deformed blade both computationally and in measurements of machined part geometries.

A representative blade geometry was designed based on inspecting an actual compressor blade to simulate similar features of the part for an accurate representation. Twist angle, chord length, camber line, and profile thickness distribution were extracted from multiple horizontal cross sections along the stacking axis, as in Figure 11B. The surrogate model does not fully entail the complexity of the original blade; however, it is used in the present study to investigate feasibility and effect of proposed probing methods. The surrogate blade model also increased machinability of the component and simplified comparative analysis of target and actual blade profiles. With regard to the former, the thicker cross section of the surrogate geometry simplified challenges associated with fixture design and machining of thin wall geometries. With regard to the latter, CMM-based measurement of the surrogate model yields less noise and minimizes vector errors due to the misalignment of normal vectors on the leading and trailing edge of sharper edge radii as in the actual industrial blades. Thus, the blade geometry was designed so to understand solely the impact of the digitization process on part accuracy. Other factors related to fixture design and measurement complexity are the subject of ongoing efforts of an applied nature. The surrogate blade has been created based on parameters and design

intent of the original compressor blade model and is shown in Figure 12. Blade cross sections along the stacking axis can be determined by two main methods described in Ref. [35], either by defining curves of concave/convex sides or by determining a mean camber line and a thickness distribution.

To model potential distortions in the blade due to service conditions, a sample of ten industrial blades were analyzed. The maximum deviation of the industrial deformed blade against the nominal blade is D_{max} at the probing z height, as in Figure 12B. The industrial blades were analyzed at the z height and their maximum deviations were averaged. The angular distortion embedded in the nominal model, and the angular distortion of the deformed model is measured as θ, as in Figure 12A. The chord length of the industrial deformed blade is short by D_{tip} at the z height due to the erosion in the trailing and the leading edge. The mean camber line is extracted from the original model and defines a skeleton and the known thickness distribution defines the concave and convex sides of the blade profile [36]. The leading and trailing edges are determined by circles with their centers on the ends of the mean camber line and a radius of the thickness at that point. The radius and profile edge thickness on the leading and trailing edges, maximum thickness, chord length and chord angle between two different cross sections were extracted from the original blade profile. These parameters are used as threshold to determine the accuracy of the cross sections in stacking axis which then be lofted to create 3D model.

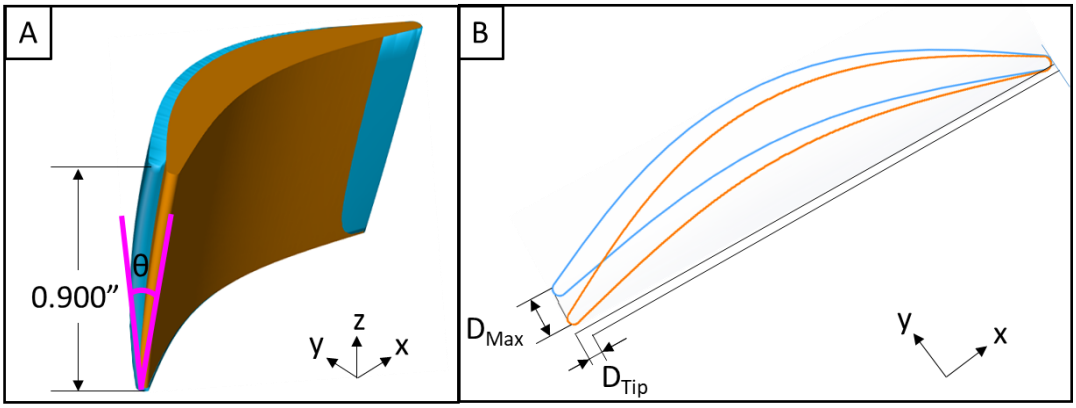

Figure 12 Designing a nominal and a deformed surrogate blade. The maximum linear deviation and angular distortion of two models are based on inspection on the actual blade scans. (A) The nominal blade (blue) is overlapped to the deformed blade (orange). The top 0.3 inch of the industrial blade, which is the only part that is serviceable, is scaled up by three times. (B) Maximum deviation (Dmax =0.030 inch) and the angular distortion (θ = 1.91 deg.) are also scaled up for machinability and visualization purposes.

1.9 Digitizing and segmenting 2-D cross sectional profile

Curvature-based segmentation (CBS) is a straightforward method for digitizing the profile of a blade geometry. In this method, each of N number of horizontal cross-sectional profiles under the weld geometry is divided into segments by its curvature. The curvature of the entire profile is calculated by taking the second derivative at each point of the profile. Median filtering is applied to the curvature values, and then the values are plotted against the position of the curvature. A threshold is then applied to split the profile into segments and is optimized so that each segment can be represented with one spline consisting of less than 7 points and 0.0005 inch of deviation (set tolerance).

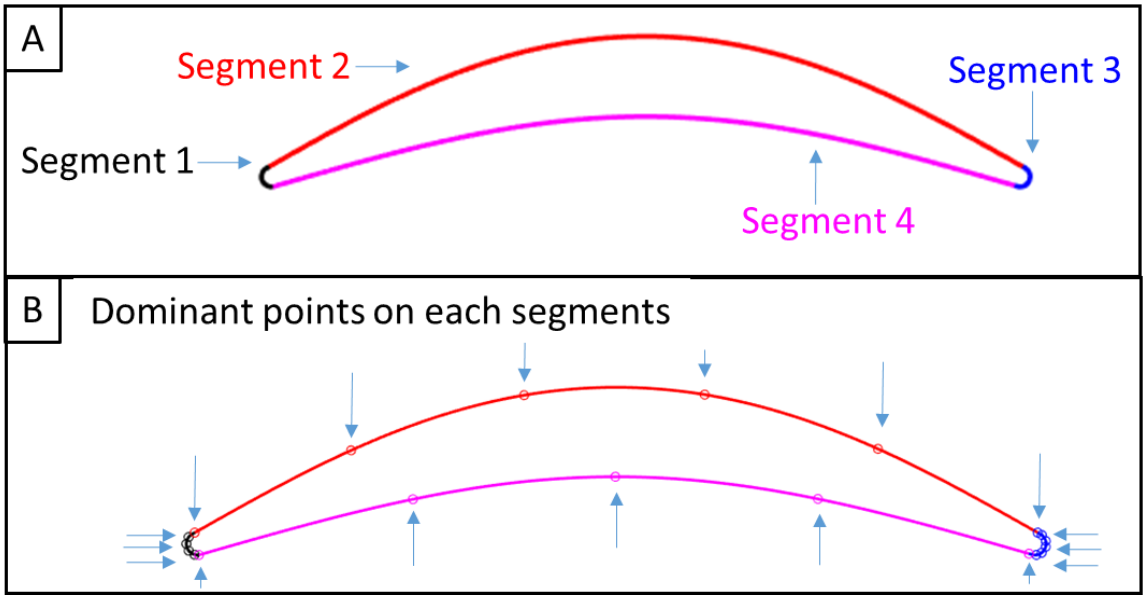

Figure 13 Illustration of segmented cross-sectional profile and dominant points to recreate each segment. (A) The 2D contour is divided into four segments. (B) Minimum number of dominant points and their positions are determined on each segment to recreate them within 0.0005 inch of tolerance.

Once the profile is split into S number of segments as shown in Figure 13A, three points are evenly distributed on the segment and a curve is reconstructed using cubic spline interpolation. If the recreated curve is deviated more than the set tolerance (0.0005 inch for the type) from the original segment, another point is added. The points are redistributed so that it is evenly distributed, and another cubic spline curve is created with those points. This iterative cycle will continue until P number of points are determined to recreate a Bezier curve that would fit the original segment within the tolerance. All S number of segments go through the same process to find the minimum number of points to reconstruct the entire profile. Figure 13B illustrates all the points distributed on each segment. This method provides curvature continuity of curves and reduced number of design parameters,

however a G1 continuity-based approach would ensures more accurate and various geometric features that are directly linked to blade geometry.

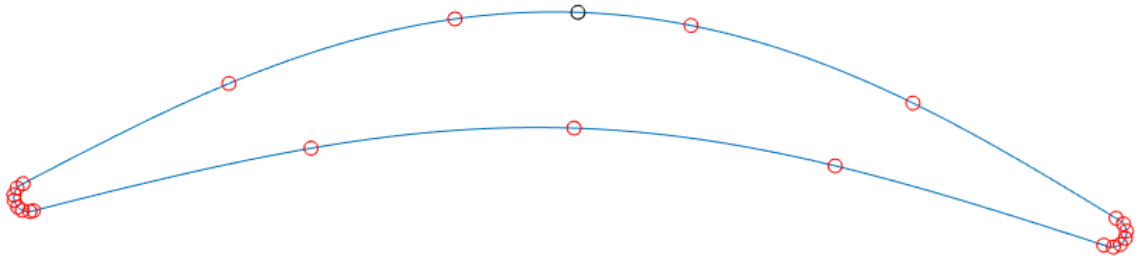

Figure 14 Profile reconstructed using points from CBS (first proposed method).

1.10 Four methods to reconstruct closed-loop profiles from segments

Four different digitization and reconstruction methods are investigated to determine the optimal solution that will provide least deviation of the reconstructed profile with minimum number of dominant points. The first method is to reconstruct a profile with a spline using all the dominant points from curvature-based segmentation, as depicted in Figure 14. G1 and G2 continuity-based methods are also used to reconstruct a spline by applying G1 and G2 continuity, respectively, where the segments are intersecting, as depicted in Figure 15B and C. The final method investigated is based on a modified curvature-based segmentation wherein the spline is modified by iteratively adding points to locations where maximum deviation occurs until set tolerance is met, as depicted in Figure 15D. The purpose of applying the above methods to reconstruction of the profile is to conserve curvature continuity along the profile after digitization. All the methods listed above will be compared against a control condition given by a dense sampling method which will be the control of the study. Once profiles are reconstructed with different

methods, they are compared against the deformed profile. The methodology for calculating maximum 2D profile deviation is described in the following section.

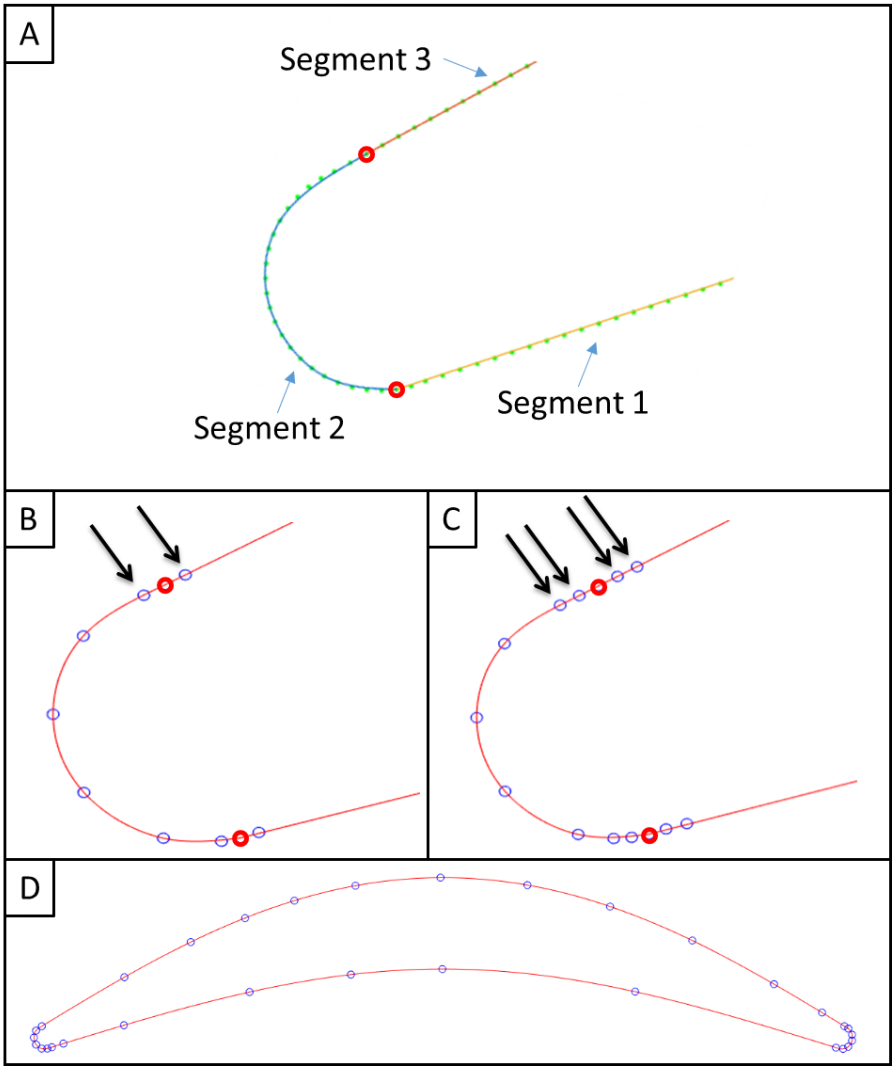

Figure 15 Dominant points used for different reconstruction methods. (A) Three segments that were that were divided based on curvature and two intersecting points between segments (red circles). (B) G1 continuity-based method is illustrated. (C) G2 continuity-based method is illustrated. (D) Local maximum control method is illustrated, and the entire profile is reconstructed (red line).

1.11 Method for calculating maximum deviation in 2D profiles

The maximum deviation is the longest distance measured between a deformed profile and a reconstructed profile. First, a deformed profile is digitized into points that are 0.0003 inch apart, as is shown in Figure 16. Three consecutive points, $P_0(x_0, y_0, z_0)$, $P_1(x_1, y_1, z_1)$, $P_2(x_2, y_2, z_2)$, are taken from the nominal profile. The starting point, P_0, can be any point on the profile. A line that goes through two points, P_0 and P_2, can be written as in Equation 10, and P(t) is a set of points that are on the line.

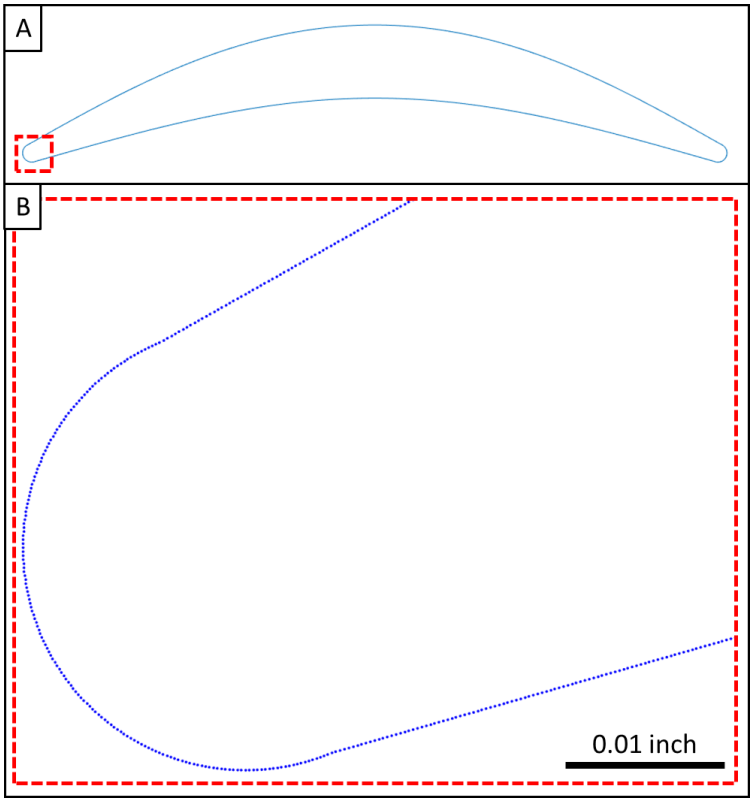

Figure 16 A deformed profile is digitized into points, and points are 0.0003 inch apart. (A) 2D horizontal profile of a deformed blade. (B) Close-up picture of the dashed red box in (A). A trailing edge of the profile is depicted as points.

$$P(t) = P_0 + \vec{v}t, where\ t \in R\ and\ \vec{v} = \begin{bmatrix} x_2 - x_0 \\ y_2 - y_0 \\ z_2 - z_0 \end{bmatrix}$$

Or,

$$\frac{x - x_0}{x_2 - x_0} = \frac{y - y_0}{y_2 - y_0} = \frac{z - z_0}{z_2 - z_0} \tag{1}$$

The spacing between points, P_0, P_1, and P_2, are so small that the line from Equation 1 is assumed to be parallel to the tangent vector of the deformed profile at P_1. Then, a plane that is perpendicular to the line and contains P_1 can be written as in Equation 2.

$$(x - x_1) \cdot (x_2 - x_0) + (y - y_1) \cdot (y_2 - y_0) + (z - z_1) \cdot (z_2 - z_0) = 0 \tag{2}$$

This plane can be assumed to be parallel to the normal vector of the deformed profile at P_1. Since the deformed profile and the recreated profile are on the same z height, the following statement is true.

$$z_0 = z_1 = z_2 \tag{3}$$

Lastly, once an intersecting point, $P_{intersect}$, between the plane from equation 2 and the recreated profile is found, the distance between P_1 and $P_{intersect}$ can be calculated. The distance can be calculated at every point on the deformed profile. Then, the maximum value of the distance is defined as the maximum deviation. Figure 17 shows three points (red circles) on a deformed profile (blue line), a perpendicular line (yellow line) that goes through P_1 and intersecting with a recreated profile (orange line) at a point, $P_{intersect}$, and a deviation between two profiles.

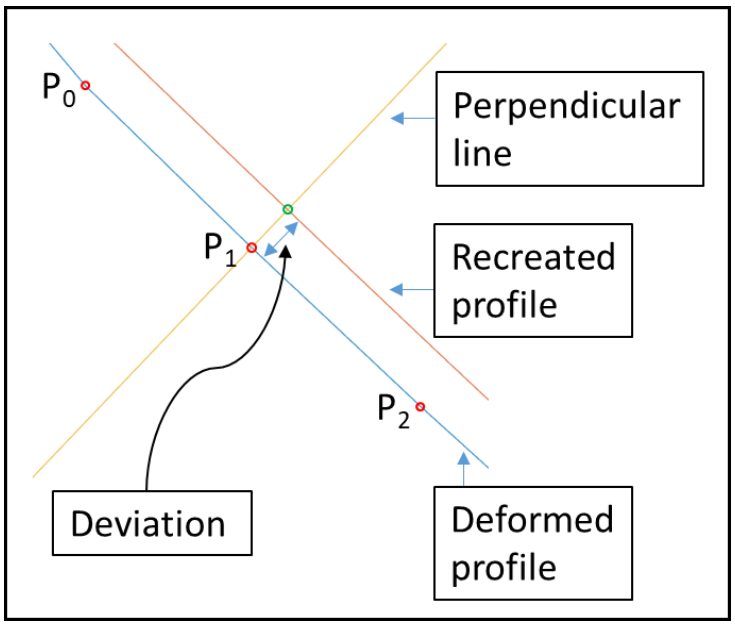

Figure 17 A representative figure to show the deviation between the deformed profile (blue line) and the recreated profile (orange line).

The 2D maximum deviation is measured to guarantee the continuity of the profile and to investigate the accuracy of each digitization and reconstruction method. The profiles will be utilized for non-rigid registration by determining the camber line (CL) and thickness distribution (TD) from the nominal and deformed profiles for each cross section. This process will be discussed in the following section. The 3D blade geometry is constructed from the 2D profiles and the 2D profile deviation will be compared against the 3D surface deviation to investigate if there is any effect of the non-rigid registration on the accuracy of the digitization methods used.

1.12 Input preparation for non-rigid registration

After 2D cross-sectional profiles in the non-weld region are recreated using the above digitization methods, a camber line of each profile must be obtained. The camber line is calculated by a profile mean line method, where the line is a set of all center points

of the largest circles that can be inscribed in the 2D blade profile in the corresponding plane. This is a plane that is perpendicular to the stacking axis of the blade and has a height of the corresponding 2D blade profile.

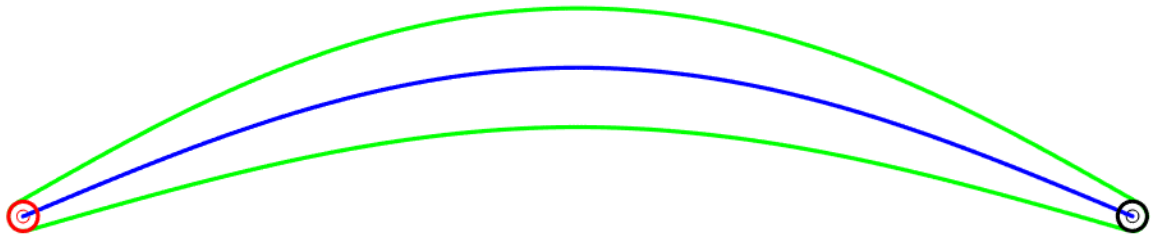

Figure 18 Camber line (blue line) is defined for a given profile (green line) with starting (black) and ending (red) points being the center of maximum inscribed circles on leading and trailing edge, respectively.

Once the camber line is obtained, maximum inscribed circles on the leading edge and the trailing edge, where their center points are located on the camber line, determine the starting and ending point of the camber line, as shown in Figure 18. The nomenclature for a nominal camber line at Z height is defined as CLnom_zi, and a deformed camber line as CLdef_zj. When the camber line is fully defined, the profile thickness is measured along the line by drawing a normal line from the camber line to the profile as shown in Figure 19A. A set of normal distances are utilized to determine the thickness distribution (TD) of the profile by fitting an H^{th} order polynomial, as shown in Figure 19B. The order of the polynomial is determined iteratively until $R^2=1$. The nomenclature for a nominal profile thickness distribution at Z height is defined as TDnom_zi and a deformed profile thickness distribution as TDdef_zj.

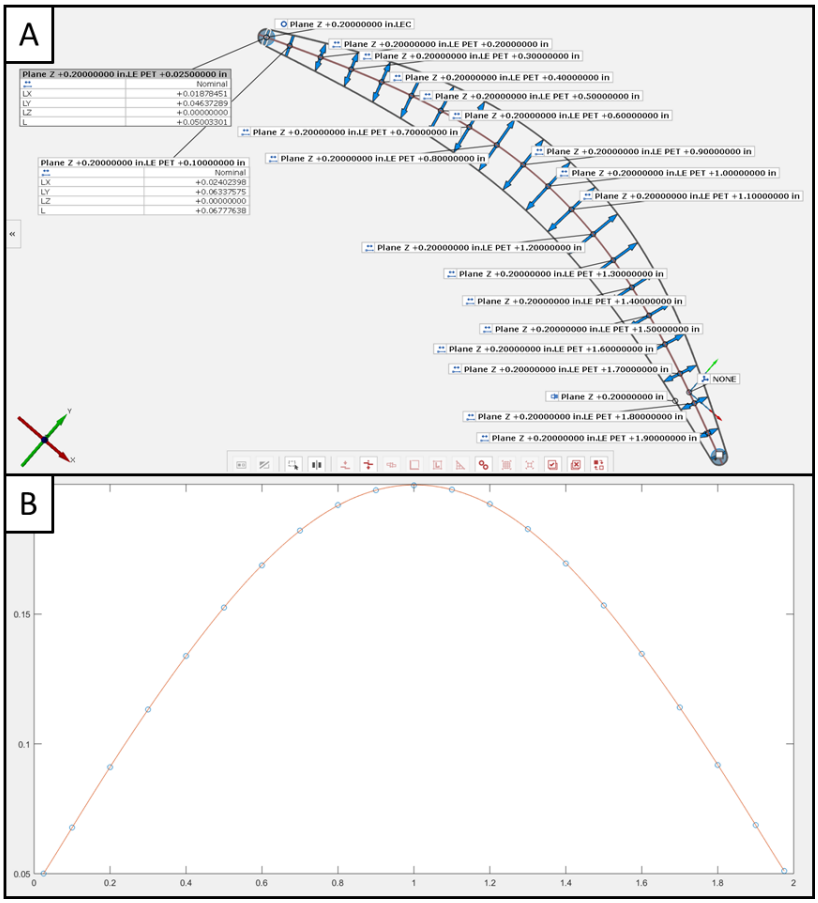

Figure 19 Cross-sectional profile with a set of thickness measurements and Hth order polynomial fit for the set of measurements.

The nominal blade geometry is non-rigidly registered to the deformed blade geometry so to adapt the blade tip geometry in the non-repair region. The inputs for the non-rigid registration are CLnom_zi, TDnom_zi, CLdef_zj, and TDdef_zj, and the outputs are CLreg_zi and TDreg_zi. CLnom_zi is the camber line and TDnom_zi is the thickness distribution, both corresponding to the nominal profile at zi height. CLdef_zj and TDdef_zj are the camber line and the thickness distribution, respectively, corresponding to the deformed profile at zi height. CLreg_zi and TDreg_zi are the camber line and thickness distribution of the non-rigidly registered profile, respectively, at zi height.

In the non-rigid registration algorithm, CLnom_zi and TDnom_zi are used to characterize the trend of the nominal blade geometry reflecting the trend of twist/angular change and chordal length variation along the stacking axis in the original modeling of the 3D blade. Nnom_zi is the number of 2D cross-sectional profiles of the nominal blade at zi height ($1 \leq i \leq K$, where i and K are positive integer). The greater N number is, the more detailed geometric pattern of the blade along the stacking axis will be established and the more accurate blade shape will be constructed. This step enables the registration method to be adaptable to any 3D blade models. Ndef_zj is the number of 2D cross-sectional profiles of the deformed blade that accounts for intentionally introduced lean and twist at zj height ($1 \leq j \leq L < K$, where j, L, K are integer, and zL is the greatest z height in non-weld region). The information from the nominal geometry provides the general trend of the blade geometry, and that of the deformed geometry guides the nominal geometry to non-rigid registration and create registered profile (Nreg_zi).

If the methodology is applied to the geometry given in Figure 22, for example, the following conditions are satisfied.

$$\begin{aligned} Nnom_{zi} &= 6;\ W = 2; \\ Ndef_{zj} &= Nnom_{zi} - W = 4 \end{aligned} \tag{4}$$

The condition can be interpreted as the following: (1) The nominal 3D blade geometry is sectioned in 6 different z heights, (2) two sections are in the weld region, and four sections are in the non-weld region, (3) only the bottom four sections of the deformed blade in non-weld region can be digitized and reconstructed. This will be utilized in non-rigid

registration algorithm to register the nominal 3D blade geometry to predict the tip geometry underneath the weld.

1.13 Non-rigid registration algorithm

Among many non-rigid registration methods, the non-rigid registration method introduced in Ref. [8] was modified and utilized for validation of digitization and reconstruction method introduced in the thesis. The non-rigid registration method used is a combination of rigid profile registration and mean line deformation. The first step minimizes the root mean squared error between the nominal and the deformed model. The second step captures and corrects variations in the geometric form of the deformed blade such as chord length deviation along the stacking axis. The rigid profile registration is also referred to as rigid body transformation which consists of translations and rotations without changing arrangements of the blade geometry [37]. In parameterizing the transformation, one of the ways to express it in terms of six parameters (p) is:

$$M = TR \tag{5}$$

where T is translation matrix:

$$T = \begin{bmatrix} 1 & 0 & 0 & p_1 \\ 0 & 1 & 0 & p_2 \\ 0 & 0 & 1 & p_3 \\ 0 & 0 & 0 & 1 \end{bmatrix} \tag{6}$$

and R is rotation matrix:

$$R = \begin{bmatrix} c_5c_6 & c_5s_6 & s_5 & 0 \\ -s_4s_5c_6 - c_4s_6 & -s_4s_5s_6 + c_4c_6 & s_4c_5 & 0 \\ -c_4s_5c_6 + s_4s_6 & -c_4s_5s_6 - s_4c_6 & c_4c_5 & 0 \\ 0 & 0 & 0 & 1 \end{bmatrix} \quad (7)$$

where p_1, p_2, and p_3 are translation in x, y, and z respectively, and s_4, s_5, and s_6 are the sines, and c_4, c_5, and c_6 are the cosines of parameters p_4, p_5, and p_6 respectively. The rotation matrix, R, is combined by multiplying three individual Euler transformations in three axis rotations in an appropriate order. Provided that cos (p_5) is not zero:

$$p_5 = \sin^{-1}(r_{13}) \quad (8)$$

$$p_4 = \text{atan2}\left(\frac{r_{23}}{\cos(p_5)}, \frac{r_{33}}{\cos(p_5)}\right) \quad (9)$$

$$p_6 = \text{atan2}\left(\frac{r_{12}}{\cos(p_5)}, \frac{r_{11}}{\cos(p_5)}\right) \quad (10)$$

where atan2 is the four-quadrant inverse tangent.

The objective is to minimize the sum of squared differences, X^2, between a deformed model and a nominal model by translating and rotating each nominal profile to the deformed profile at the same height. Twist is calculated by comparing the camber lines in both models and is defined as planar rotation. At each iteration of the rigid registration, models are evaluated using the current parameter values. The iterative closest point algorithm is utilized to align the point sets in the nominal blade to the deformed blade. The number of iterations can be given to the algorithm or it can run until the error in the sum of squared differences between iterations becomes less than 0.1%. Then all the parameters

are saved to be used for (N-W) profiles. The transformation matrix for the profiles that are in weld region are interpolated using the transformations in non-weld regions.

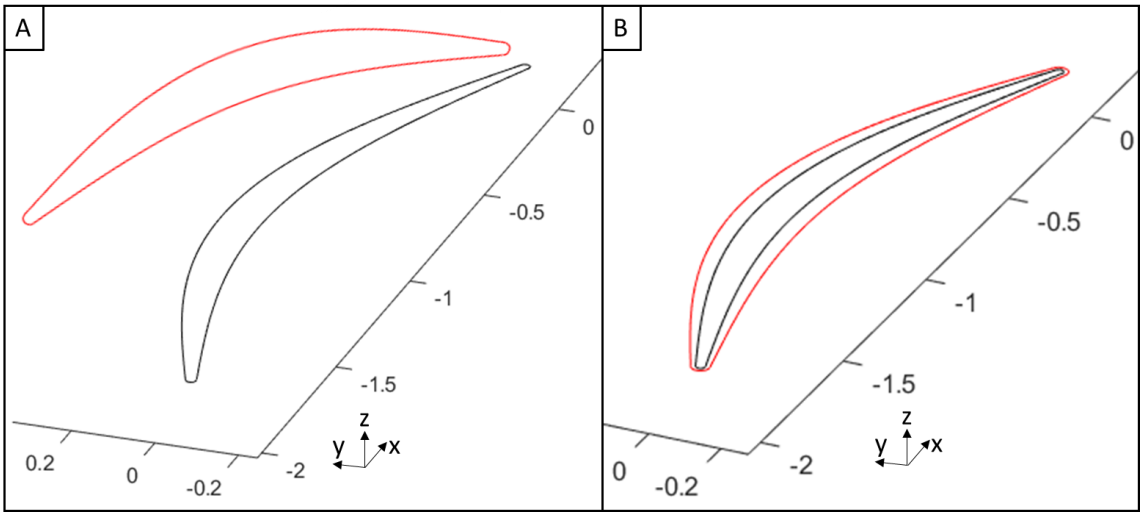

Figure 20 Representative image of rigid transformation. (A) Nominal profile (red line) is not aligned with deformed profile (black line). (B) Translation and rotation are applied to nominal profile to be aligned with deformed profile.

A representative image of rigid transformation of a nominal profile to a deformed profile is depicted in Figure 20. A nominal profile is not aligned with a deformed profile in Figure 20A. An appropriate transformation matrix is applied to minimize the sum of squared differences between two profiles. Registration is not complete because the deformed profile has shorter chord length and smaller thickness throughout the entire profile due to material erosion, as in Figure 20B.

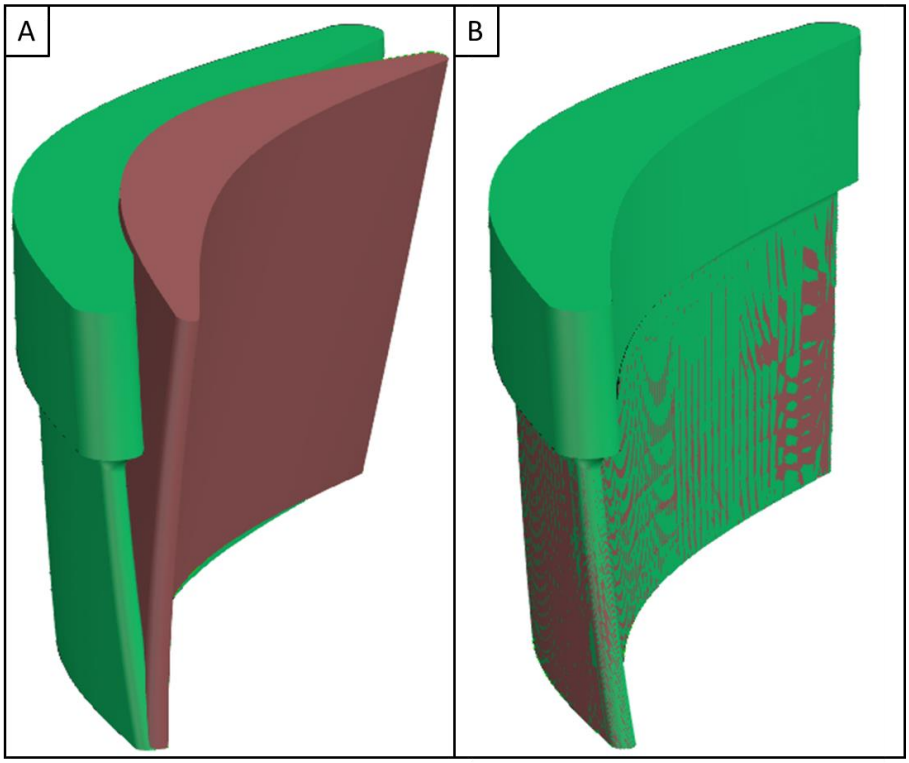

Figure 21 Complete non-rigid registration of nominal blade (brown) to welded deformed blade (green). (A) Before non-rigid registration. (B) After non-rigid registration.

Mean line registration accounts for any deviation (D_{tip} in Figure 12B) of warping in blade geometry. After rigid transformation, the control points of camber lines from deformed profiles are examined and used to deform nominal camber lines in profiles in corresponding heights. The camber lines of the profiles in the weld region are interpolated using non-weld region profile camber lines as is done in rigid body transformation. Once the mean line is registered for each height of the profile, thickness distribution data from the deformed profiles are applied to nominal profiles. This accounts for regions of the blade that have less thickness than the nominal blade due to the wear. With multiple steps in non-rigid registration, N profiles of nominal blade geometry are registered to (N-W) profiles of deformed blade, and the 3D model is fully registered as in Figure 21B.

The main distinction between the present approach and that of Ref. [8] is utilization of digitization method. The method in Ref. [8] defined a deformed blade so the camber line and thickness distribution for the non-weld region were known. The proposed method in this thesis digitizes a deformed 3D blade geometry, recreates cross-sectional profile of the non-weld region, and extracts camber line and thickness distribution information for non-rigid registration of the nominal blade geometry. The given 3D blade geometry is sectioned perpendicular to the stacking axis and 2D profiles in the non-weld are digitized and reverse engineered to extract camber line and thickness distribution.

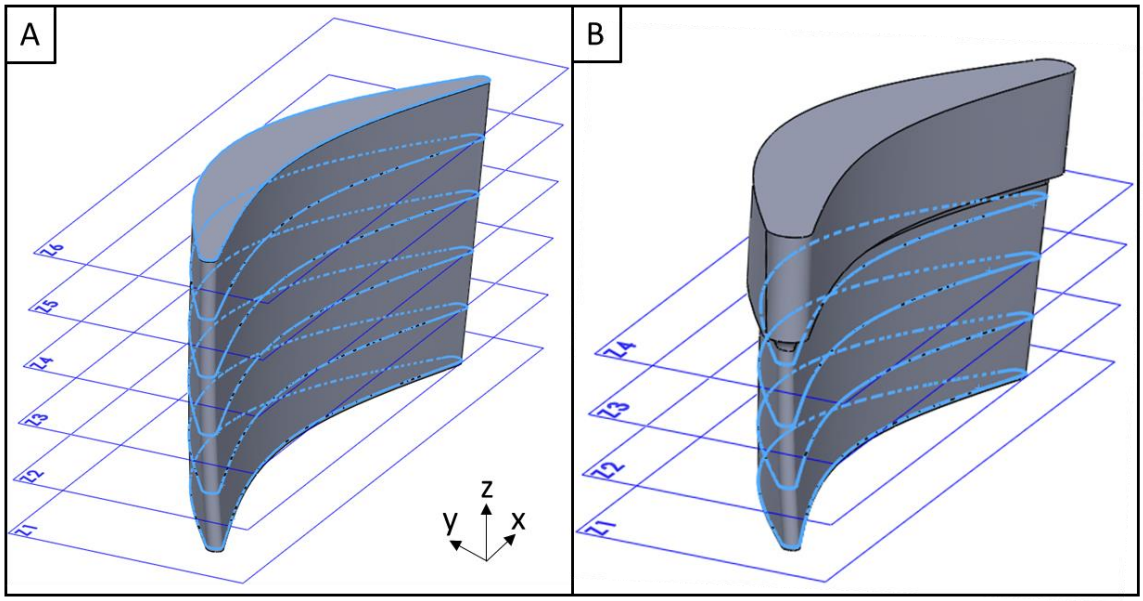

Figure 22 A representative figure of cross-sectional blade profiles in (A) nominal blade and (B) deformed blade when there are 6 sections made in nominal blade and 4 sections in non-weld region (Nnom_zi = 6, W = 2, Ndef_zj = 4).

To validate the strategy, several sets of nominal blade geometries and deformed blade geometries were generated. The nominal blade geometry was sectioned with Nnom_zi planes perpendicular to the blade stacking axis (shown as the Z axis in Figure 22A), this creating 2D cross-sectional blade profiles to assess the trend in twist/angular

change and chord length deviation, as in Figure 11C and Figure 11D. Among these Nnom_zi profiles (from plane Z1 to Z6 in Figure 22A), W indicates the number of 2D blade profiles (Z5 and Z6 plane in Figure 22A) of the nominal blade in the weld region and used to register the nominal blade to the deformed blade for interpolating the tip geometry. The surrogate blades are digitized using (Nnom_zi – W) cross-sectional profiles in the non-weld region (Figure 22B).

1.14 Probe path, additive toolpath and subtractive toolpath creation

The ultimate purpose of registering a nominal blade to a deformed blade is to implement the strategy to an actual digitizing, registering, and machining setup that could be utilized in a hybrid manufacturing environment. An additive toolpath, a probe path, and a machining toolpath have been created for a 5-axis machine (Mazak VC-500AM) shown in Figure 24. The additive toolpath and the probe path were creating using a commercial CAM software.

1.14.1 Toolpath for additive manufacturing

An additive toolpath (Figure 24A, C) was not implemented on the machine in order to eliminate any unforeseen errors from the process that could affect digitization process. Nevertheless, the additive toolpath was created so to validate the welded tip geometry that was used as the deformed model and to show the feasibility of a completed hybrid blade tip repair process in simulation. In Figure 24, a green line represents a laser coming from

the source, and a yellow tip represents a laser bead that is 0.04 inch in diameter. An additive toolpath is created along the profile of the blade perpendicular to the stacking axis with

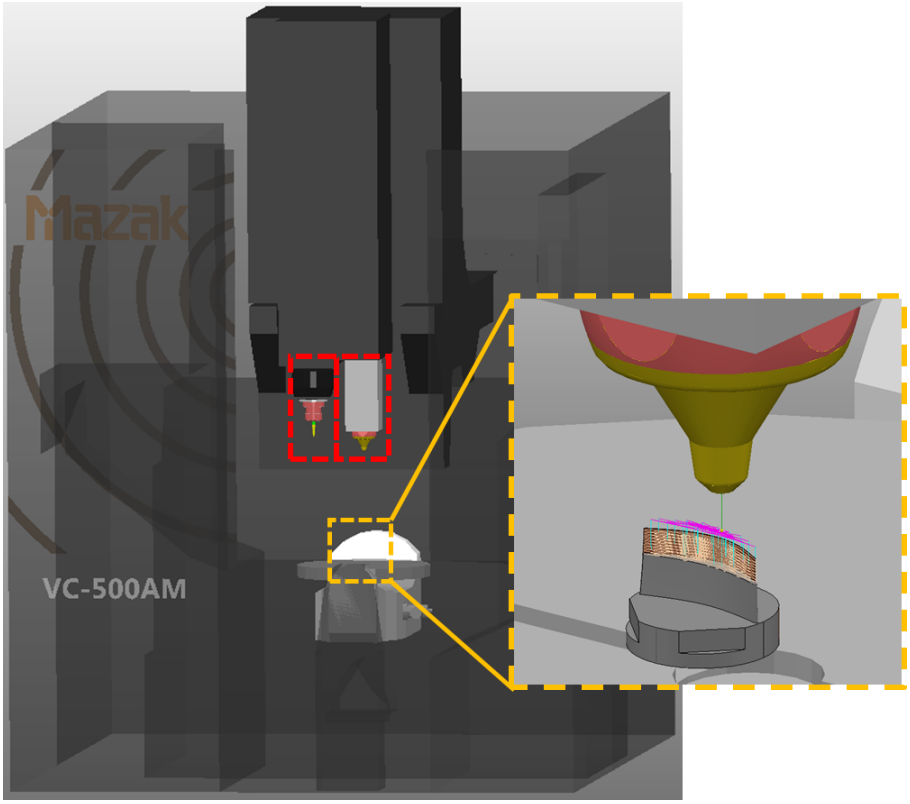

Figure 23 Mazak VC-500AM 3D model with subtractive tool head in the left red box and additive laser head in the right red box. Yellow box shows an example of additive toolpath for welding the blade tip.

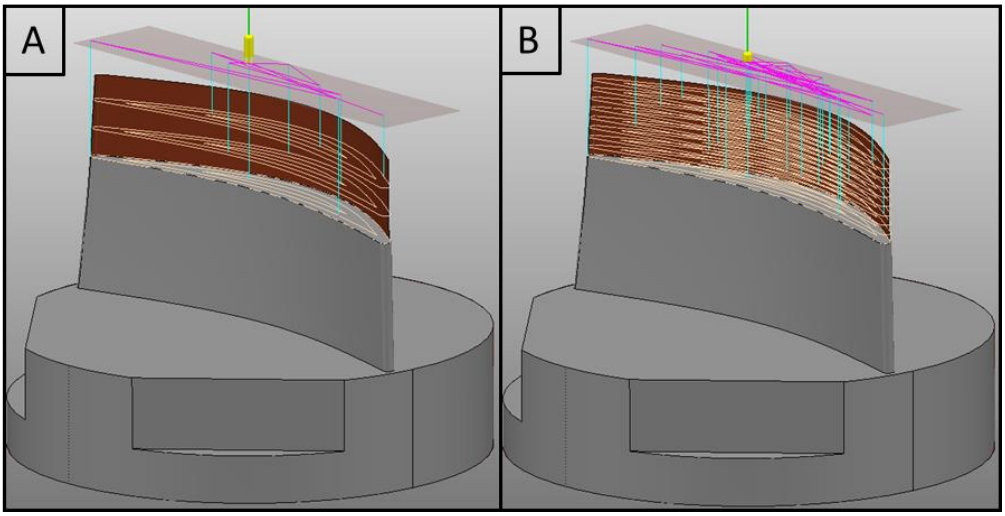

Figure 24 Additive toolpath created in CAM software. (A) additive toolpath created along the blade profile with 3mm layer thickness, (B) additive toolpath with 1mm layer thickness.

0.04 inch step over offset from the blade profile. Layer thickness is set as 0.12 inch to show a clear individual additive toolpath in Figure 24A and is set as 0.04 inch in Figure 24C, which represents a more realistic additive toolpath. Normally, a layer thickness of 0.12 inch is too thick and will result in poor dimensional accuracy. The additive toolpath is simulated with a commercial CAM software on the repair region of the blade where Figure 25A shows a build three layers into the process and Figure 25B shows a completed weld tip. Since the toolpath follows the boundary of the blade profile, it is likely to have at least 0.02 inch of excess material normal to the surface of the tip geometry.

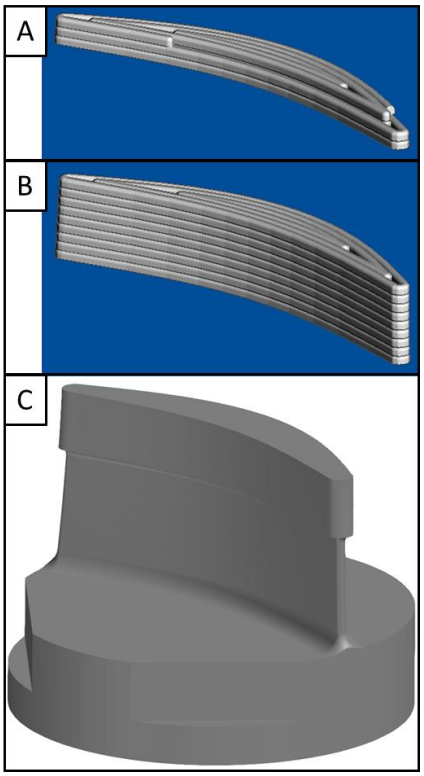

Figure 25 Additive toolpath in simulation and welded blade geometry to best represent the weld. (A, B) weld is being deposited using additive toolpath from Figure 24B, (C) a welded blade geometry reflecting the weld simulated through simulation.

1.14.2 Probe path for registration of deformed welded blades

If the deformed blade was to be welded in a hybrid manufacturing setting, the machine must probe the non-weld region of the blade to register the deformation of the blade. When the digitization method is ultimately implemented, the quality of the final product is not only dependent on the digitization and registration algorithm but also dependent on the accuracy of probing the blade. Two main factors that affect the probing accuracy are the approach vector, which is a normal vector from the surface, and contact points on the surface. The machine will first align the part either by probing relative XYZ

planes that serve as origin for the part (Figure 25A) or the blade will be installed in a fixture that has been already registered in the machine. Then horizontal profiles will be probed with the appropriate planned probe path, as in Figure 25B.

It is important to note that the deformations that exist on the blade surface will generate different approach vectors and surface locations than the planned probe path as is depicted in Figure 27. This error cannot be compensated unless the deformed blade is scanned with a structured light scanner and have its coordinate system matched with that of the hybrid machine platform, both of which are not generally practical from a rapid repair production stand point. This vector and position error should be addressed to eliminate unwanted 2D profile and 3D surface deviations that might be present. In this regard, to isolate the effect of the digitization algorithm alone, the present study idealized probe-related data from simulation. Nonetheless, probe paths have been generated to validate accessibility of the probe to the probe points that the digitization method produces as shown in Figure 26. The coordinate orientation and origin of the part has to be aligned with those of the machine (Figure 26A), and then probing cross-sectional points in the non-weld region at multiple Z height has to be performed (Figure 26B). Probing the deformed blade is a necessary step before welding the tip and machining the tip in order to maximize time and material efficiency [8].

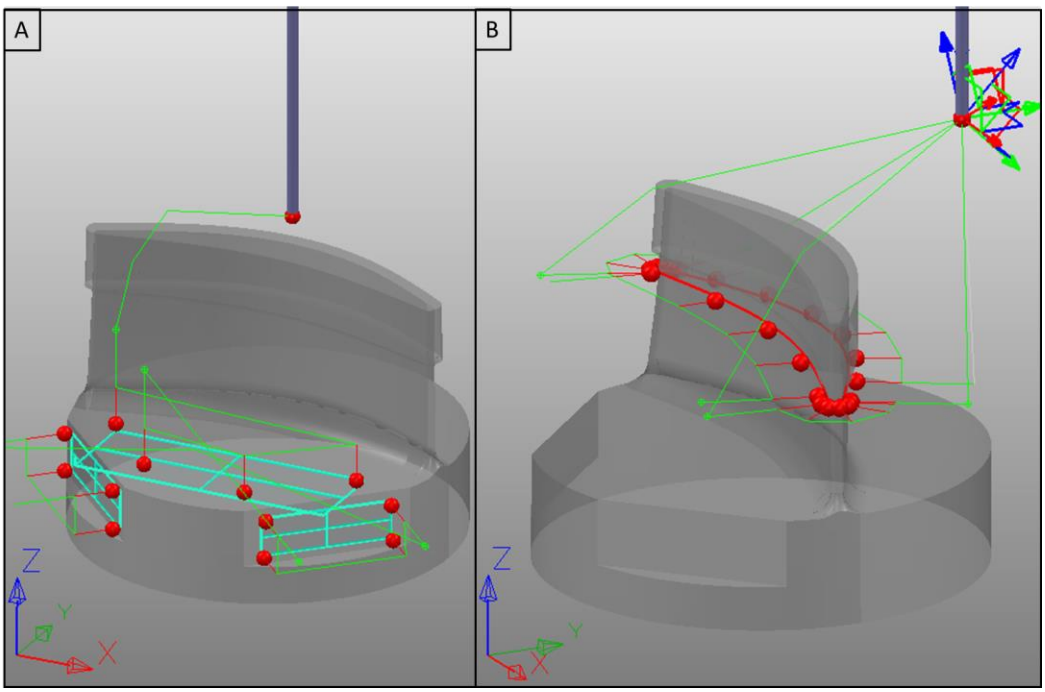

Figure 26 Probe paths created for a machined blade with weld geometry. (A) Probe path for part alignment. (B) Probe path for blade deformation registration on non-weld region.

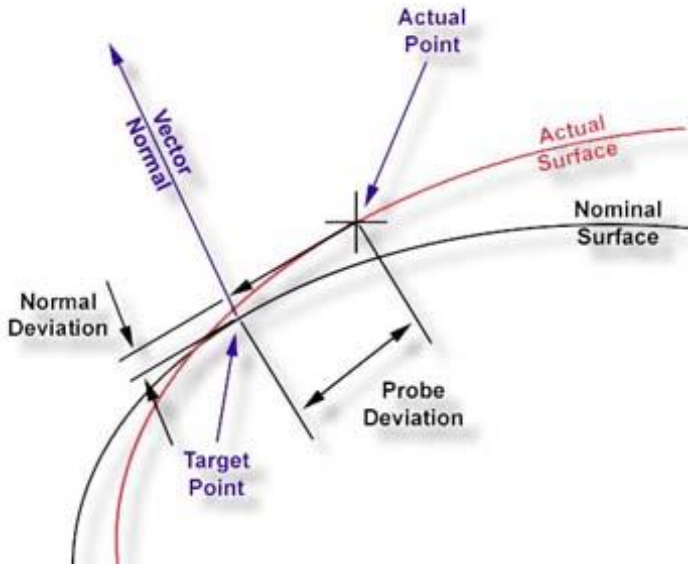

Figure 27 Normal and probe deviation that could exist in deformed blade in on-machine probing.

1.14.3 Toolpath for welded blades and registered blades

Welded deformed blade geometries were produced by machining. The machining toolpaths (Figure 28A) for welded blades were carefully designed to machine the weld geometry as close as possible to how it was designed especially where the weld and the non-weld region intersect. Five different toolpaths for machining the weld geometry were created based on the non-rigidly registered models that utilized five digitization methods. Once a welded deformed blade was machined, a weld blending toolpath (Figure 28B) was executed on a single machine setup to avoid alignment errors in the machining process so that any blendline steps would be due to the digitization method and physical response during machining. The blendline region of the completely machined blades are measured with a coordinate measurement machine for validating the result of the simulation.

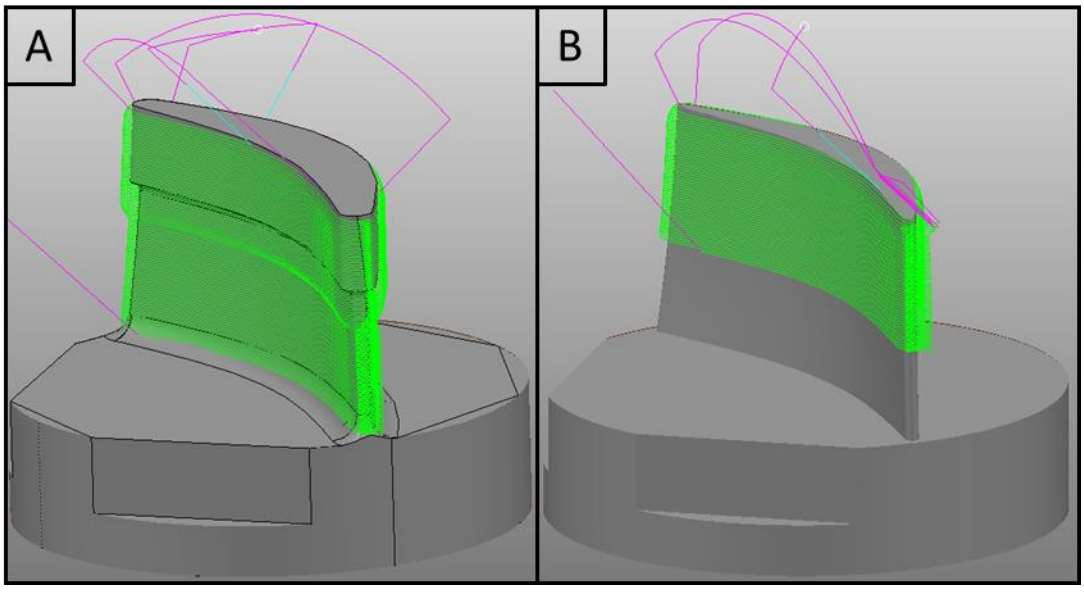

Figure 28 Machining toolpath for (A) welded blade geometry and (B) machining the welded geometry.

RESULTS AND DISCUSSION

The nominal and deformed surrogate blade geometry was used to validate the effect of digitization approaches – including dense sampling (DS), curvature-based segmentation (CBS), G1/G2 continuity, and local control approaches – on accuracy of non-rigid registration. The horizontal 2D profiles in the non-repair region of the deformed blade were digitized and used to non-rigidly register the nominal blade to the deformed blade as shown in Figure 22. 2D profile deviation and 3D surface deviation were analyzed and tabulated. The final non-rigidly registered blade geometry was then used_to create machining toolpaths for remanufacture of the blade geometry and compared against the simulated results. In the case of certain surface deviation between the deformed blade and the final registered blade, quality defects would result as this deviation would create a measurable blendline step and/or surface deviation.

1.15 Deviation analysis of digitization methods on 2D profile and 3D surface

Blade cross-section profiles (Zn, maximum height of Zn < 0.411inch, n >= 2) of the deformed blade in the non-repair region were digitized using the DS (control), CBS (method 1), G1/G2 continuity (method 2 and 3), and local profile control (method 4) digitization approaches. A representative figure of profile deviation is shown in Figure 17, and the resulting maximum profile deviations are calculated using normal vectors from the horizontal 2D profile towards the digitized profile and then are tabulated for all five approaches in Table 1.

All the profiles that are digitized and reconstructed in the non-weld region are used to non-rigidly register the corresponding profiles in the nominal blade. A registered 3D geometry is constructed using the registered profiles, and the surface deviation of the registered blade was calculated against the deformed blade. The maximum surface deviations in 3D blade geometries are tabulated in Table 1 and plotted in Figure 29.

Table 1 Deviation analysis on 2D profiles and 3D surfaces for multiple methods ('DS' and 'CBS' refer to 'dense sampling' and 'curvature-based segmentation', respectively).

Method		Deviation in 2D profile (inch)		Surface deviation in 3D models (inch)	
	Number of points	Maximum deviation	Average deviation	Maximum deviation	Range of deviation
DS	1047	2.5×10^{-5}	9.7×10^{-7}	-1.6×10^{-4}	$-1.6 \times 10^{-4} \sim 6.8 \times 10^{-5}$
CBS	21	3.4×10^{-3}	1.1×10^{-3}	4.3×10^{-3}	$-3.7 \times 10^{-3} \sim 4.3 \times 10^{-3}$
G1 cont.	29	3.9×10^{-3}	1.0×10^{-3}	3.9×10^{-3}	$-3.8 \times 10^{-3} \sim 3.9 \times 10^{-3}$
G2 cont.	37	3.7×10^{-3}	1.0×10^{-3}	4.3×10^{-3}	$-3.9 \times 10^{-3} \sim 4.3 \times 10^{-3}$
Local max. control	32	4.7×10^{-4}	1.3×10^{-4}	5.1×10^{-4}	$-1.5 \times 10^{-4} \sim 5.1 \times 10^{-4}$

The deviation that is present in 2D profile digitization carries over to and affects the surface deviation. Dense sampling method (named as DS in Table 1) collects the largest number of probing points resulting the best reconstructed 2D profile with the smallest

maximum deviation in both 2D profile, 0.000025 inch, and 3D surface, -0.00016 inch. A small increase in the deviation occurs when non-rigid registration is applied, however, it is still within the limit of the set tolerance which is 0.0005 inch. The average deviation is calculated by dividing the sum of all the deviations from each individual probing point by the number of probing points.

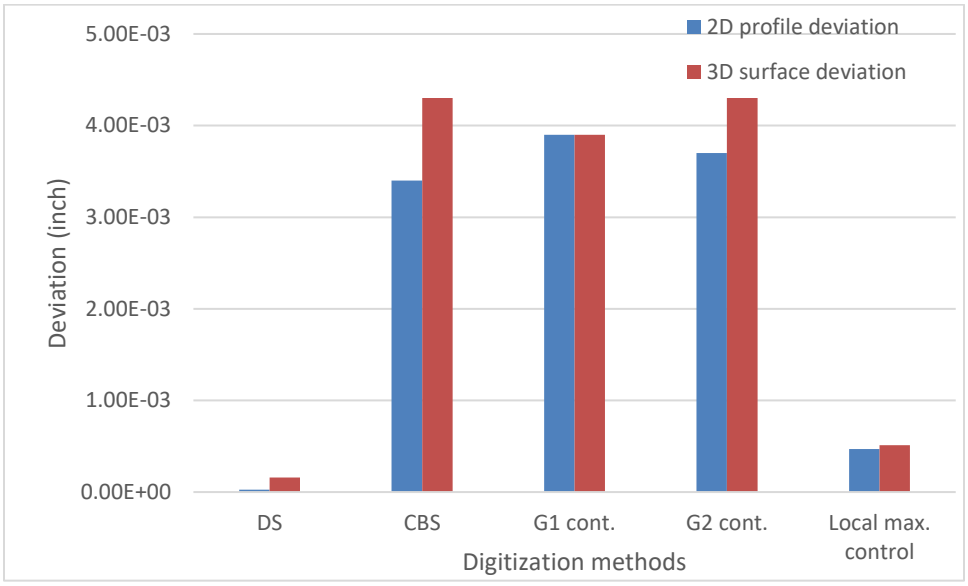

Figure 29 Deviation of 2D profile and 3D surface between a deformed blade and a registered blade.

The probe-based inspection time using a Renishaw RMP600 high accuracy machine probe was calculated to be 15 minutes for the DS method and 30 seconds for the CBS method. Regardless of its accuracy, the dense sampling method is impractical to implement in the production line due to the time required. It could only serve as the control group of the study to prove that when enough points are acquired, a 2D profile with negligible deviation could be constructed. Nonetheless, this resulted the smallest deviation in reconstructed dimensional accuracy in both 2D profile and 3D surface geometries.

To reduce the amount of probing points, curvature-based segmentation strategy was applied to the 2D profile. Once the profile is segmented at the appropriate points where the change in tangent vectors of the profile is drastically changing, each segment is assigned with probing points which can reconstruct the segment with a set tolerance of 0.0005 inch. The segments alone could not be used because only G0 continuity can be guaranteed between segments, which can severely affect reconstruction of a complete profile such as pointy intersecting region between segments. Thus, curvature-based segmentation method creates one spline reconstructed from all the probing points from each segment satisfying continuity along the profile.

As segments are joined with their probing points, the intersecting points are experiencing abrupt change in tangent vector of the profile. This leads to big jump in maximum deviation from DS to CBS method from 0.0005 inch to 0.0034 inch. When this profile is taken into non-rigid registration of the nominal blade, the registered blade resulted in 0.0043 inch of surface deviation which is 0.0009 inch higher than the profile deviation. Compared to the DS method, the CBS method can be implemented using 21 probing points and take only 30 seconds to probe one horizontal profile, however, the accuracy does not satisfy the standard. The 2D deviation is further analyzed to investigate the origin of the deviation and to reduce the deviation.

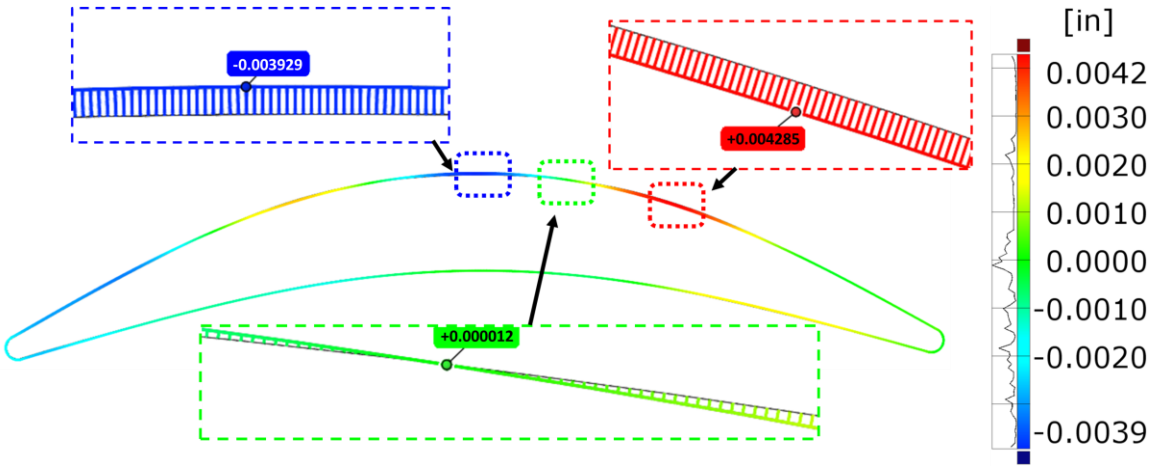

Figure 30 Reconstructed blade profile (black line) using G2 continuity-based method compared on deformed blade (colored line). Positive maximum (red box), negative maximum (blue box), and transition point (green box) are zoomed in. Distribution of deviation is drawn as a histogram next to the color scale.

Further analysis took place to investigate where the error is occurring or accumulating. When a profile is being non-rigidly registered, the camber line and thickness distribution data is determined as described above. There is no error in acquiring the data, but when it is registered and reconstructed, profile deviation is observed as periodic as shown in Figure 30. The deviation trend is more dramatic on the convex side of the blade. There are two possible reasons for the trend: (1) the change in curvature in the intersecting point is not controlled and (2) when the thickness of the profile is being measured, the line that goes through the profile is not necessarily perpendicular to the camber line. To reduce the deviation caused by CBS method, G1 and G2 continuity-based methods are tested as the second and the third method to recreate the spline for the profile.

G1 and G2 continuity-based methods are attempted to reduce the maximum deviation that occurs in the CBS method as the method joins multiple segments. When curvature-based segments are joined together, they are only guaranteed to satisfy G0 continuity as it is shown in Figure 31B. In a CBS method, a spline is drawn from the points

of the segments, so there are no unsmooth edges in the intersecting point. However, since the segments are divided by their curvature from one segment to another, the intersecting point may experience a drastic change resulting more deviation. To alleviate the abrupt curvature change, an attempt to create G1 and G2 continuity at the intersecting point were tried by adding points adjacent to the point.

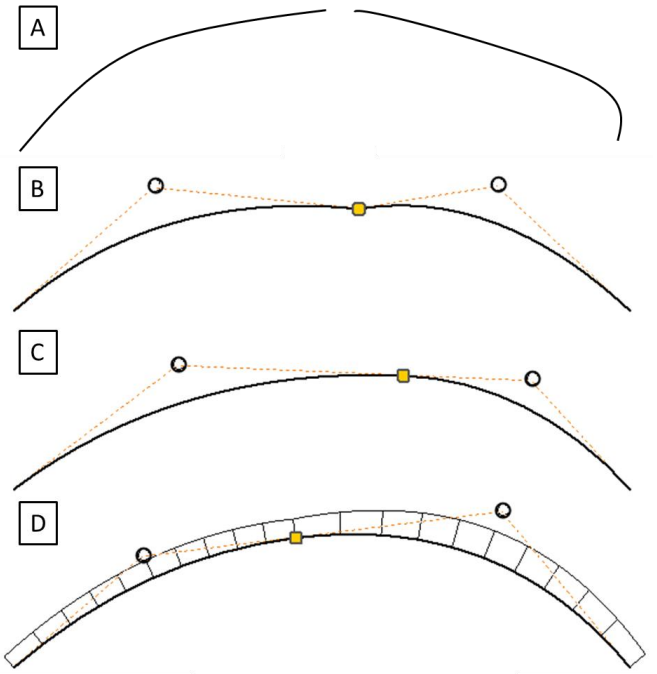

Figure 31 Degree of continuity. (A) no continuity between two lines, (B) G0 continuity, (C) G1 continuity, (D) G2 continuity [38].

A spline was generated with additional points, however, the maximum deviation still increased from 0.0034 inch to 0.0039 inch and 0.0037 inch for G1 and G2 continuity, respectively. The surface deviations using those two digitization methods reflect same or higher deviation than the profile deviation as it is shown in the bar graph in Figure 29. This is the periodic deviation that existed in the CBS method and has not been attenuated. To resolve the deviation larger than the tolerance required, local control of maximum deviation method is introduced as a fourth method.

Table 2 Change in deviation after each iteration in reconstructing 2D profile from probing points.

Iteration	Number of points	Deviation
0	21	3.4×10^{-3}
1	22	2.0×10^{-3}
2	23	3.0×10^{-3}
3	24	1.1×10^{-3}
4	25	0.8×10^{-3}
5	26	4.9×10^{-3}
6	27	0.9×10^{-3}
7	28	1.3×10^{-3}
8	29	1.8×10^{-3}
9	30	0.7×10^{-3}
10	31	5.01×10^{-4}
11	32	4.70×10^{-4}

Controlling local maximum deviation method places probing points to where the maximum deviation occurs in each iteration so that when a spline is drawn through the probing points, it would reduce the maximum deviation of the whole profile. The values of maximum 2D profile deviation are tabulated in Table 2 and graphed in Figure 32. The initial model at 0 iteration is CBS method that has 21 probing points and profile deviation of 3.4×10^{-3}. At each iteration, one point is added to the location where maximum deviation occurs. A spline is constructed having one more point than the previous iteration, and the maximum deviation is measured again. When a point is introduced at the local maximum deviation, it reduces the maximum deviation to zero because the constructed spline goes through it, however, it could possibly constraint adjacent region to have larger deviation than the previous iteration.

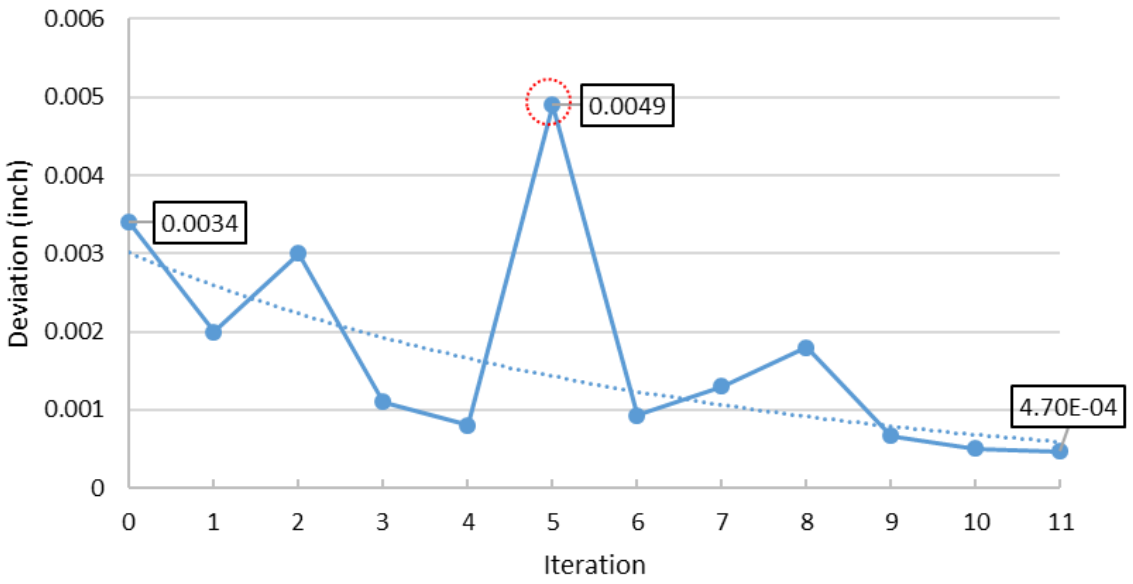

Figure 32 Change in maximum 2D profile deviation as a point is added each iteration. An abnormally large maximum deviation is created at 5th iteration (red circle) of placing points at maximally deviated location. Dotted line is an exponential trendline fitted to the data.

Adding points at the location where maximum deviation exists does not guarantee lowering of the maximum deviation in all cases as one can see from Figure 32. The deviation fluctuates, and it cannot be predicted before it is place and a spline is constructed including the added point. The second iteration (Figure 33A) and the fifth iteration (Figure 33B) show greater increase after the point is added, because the added point constrained the spline construction and created more linear segments where it needs a curved contour as it is shown as red arrows in Figure 33A, B.

After 11 iterations, the fourth method successfully finds 32 points that can be used to create a spline with less than a set tolerance of 0.0005 inch. Although the deviation seems to increase at a certain iteration cycle, the overall trend of deviation decreases as more points are added. All existing probing points and added points are marked with red

circles, and a constructed spline (red line) is hid behind the deformed profile (green line) in Figure 33C.

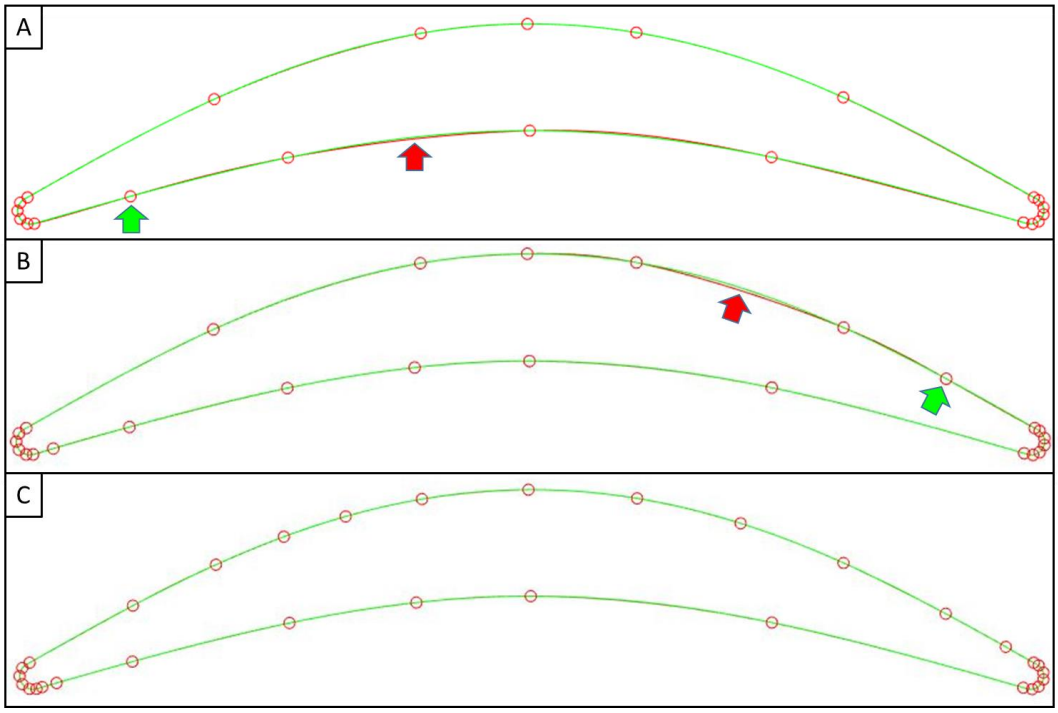

Figure 33 Deformed profile (green line) overlaid on constructed spline (red line) from probing points (red circles). Green arrow represents where the point is added, and red point represent the maximum deviation due to the added point. (A) second iteration, (B) fifth iteration, and (C) eleventh iteration whose tolerance is less than the set tolerance.

1.16 Deviation comparison between simulated and machined blades

Simulated surface deviations between non-rigidly registered blades and deformed blades are compared with measured blendline heights in machined blades. The registered blades are utilized to create toolpaths, and machined blades are measured at the blendline region using a coordinate measurement machine, Zeiss Micura CMM, to quantify the blendline heights.

From Table 1, the non-rigidly registered 3D blade geometry that was registered using the DS method and the local maximum control method resulted in significantly smaller surface deviations, -1.6×10^{-5} inch and 5.1×10^{-4} inch respectively, compared to that of the CBS, G1 and G2 continuity methods, which resulted in surface deviations of 4.3×10^{-3} inch, 3.9×10^{-3} inch, and 4.3×10^{-3} inch, respectively. The corresponding 2D profile deviations for these methods were similar to that of 3D surface deviations as is shown in Table 1 and Figure 29.

The surface deviation in the blendline region is visualized to characterize the distribution of the deviation in 3D geometry as shown in Figure 34. Positive surface deviations (red color in the error bar) indicate unmachined material remaining, and negative surface deviations indicate machining too much into the parent material. For the DS-based digitization approach, maximum surface deviation of -1.6×10^{-4}inch occurred on maximum surface deviation of 5.1×10^{-4} inch occurred both on the concave and convex side. These deviations are shown in Figure 34 A and E. In comparison, the CBS-based approach and G1/G2 continuity-based approach resulted in a maximum surface deviation of 4.3×10^{-3}inch, 3.9×10^{-3}inch, and 4.3×10^{-3}inch on the convex side of the blade profile as shown in Figure 34 B,C,D. From the figure, the surface deviation explicitly depicts a periodic deviation on the blade surface for both digitization approaches.

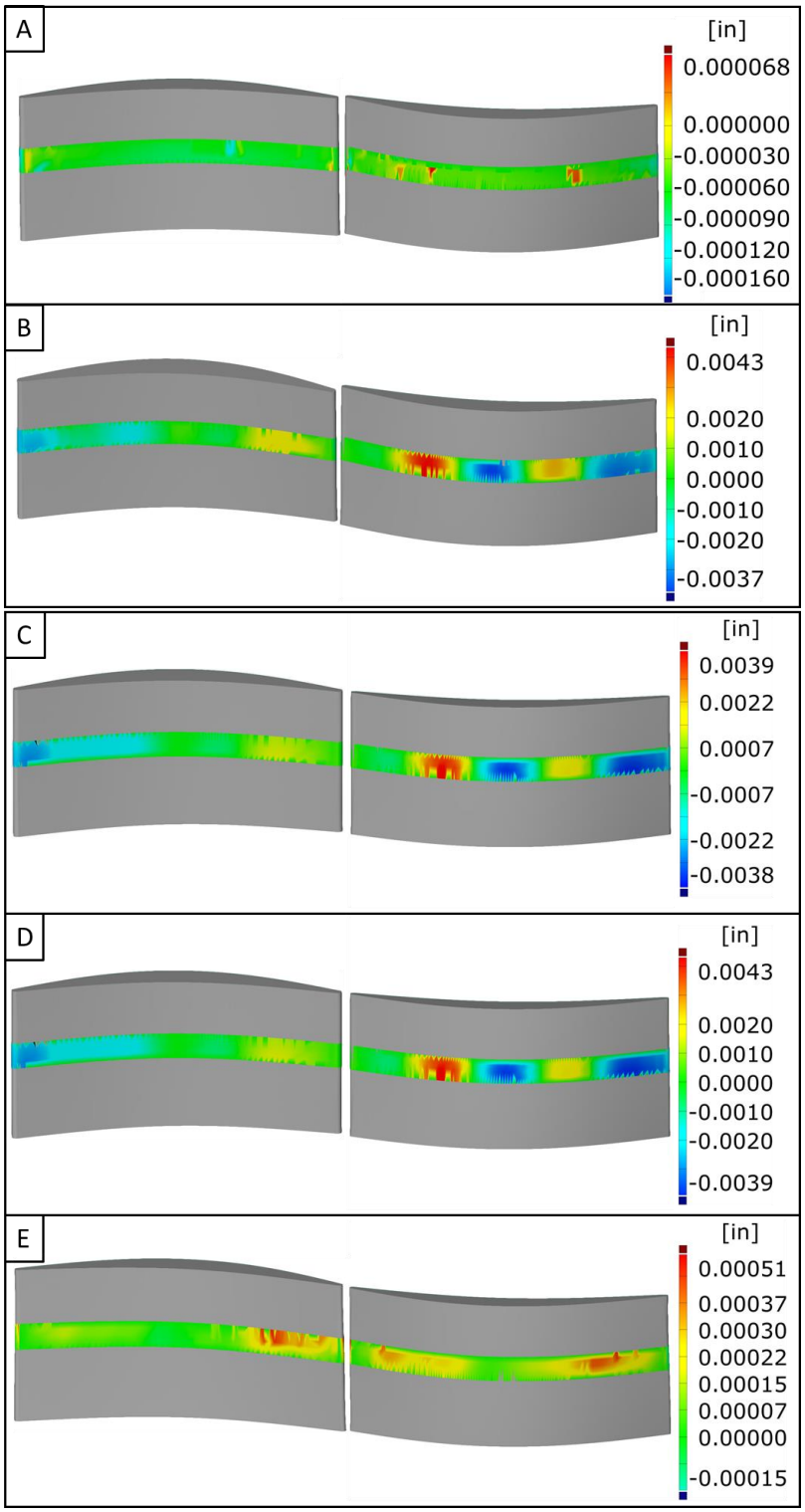

Figure 34 Surface deviation is inspected on non-rigidly registered model against the deformed model in the blendline region. Concave and convex side are shown on the left and right, respectively. The surface deviation results are from different digitization methods: (A) dense sampling (control), (B) curvature-based segmentation method, (C) G1 continuity, (D) G2 continuity, and (E) local maximum control.

This periodic deviation on the blade surface is the product of the digitized profile because the deviation characterized in the 2D profile shown in Figure 30 is in congruency with that of the 3D surface deviation trend. This proves that the error from 2D profile digitization and reconstruction directly propagates to the non-rigid registration process. In other words, local maximum control method successfully digitizes the deformed model and non-rigidly registers the nominal blade to the deformed model at a set tolerance.

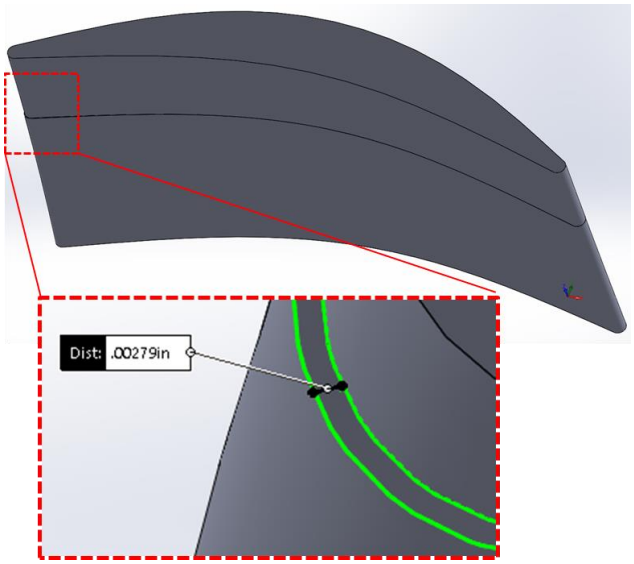

Figure 35 An example of blendline on the blade in simulation. Red dotted box is a close-up of the blendline height in the trailing edge.

In the blade geometry, the blendline region is defined within the range of 0.411 inch ≤ z height ≤ 0.561 inch (Figure 7b) which was referenced to the z height of where the bottom of the repair region and non-repair regions intersect, and where blendline defects are most likely to occur. An example of a blendline that is generated in simulation is depicted in Figure 35. To investigate the capability of the simulation approaches to predict the surface deviation and blendline geometry, a set of 5-axis machining tests were performed using

five profile digitization and reconstruction approaches with the registration algorithm. A Mazak VC-500A/5X vertical machining center was utilized to machine surrogate blade geometries in Al6061-T6 workpieces with 3/8 inch diameter 6 flute solid carbide end mill and 3/16 inch diameter 6 flute solid carbide tapered ball end mill. First of all, the deformed welded geometry was machined from billet stock. The blade geometry was then digitized using the proposed methods including DS, CBS, G1/G2 continuity, and local maximum control approaches. Then, toolpaths were generated based on the non-rigidly registered blade geometry. The blades were machined and finish blended on a single machine setup so to eliminate any registration errors that might exist in the machining process. In this regard, any profile deviations or blendline defects would be due to the digitization approach and physical response during machining only. Figure 36 shows the inspection method in 10 different locations on the blade used to determine the blendline step geometry.

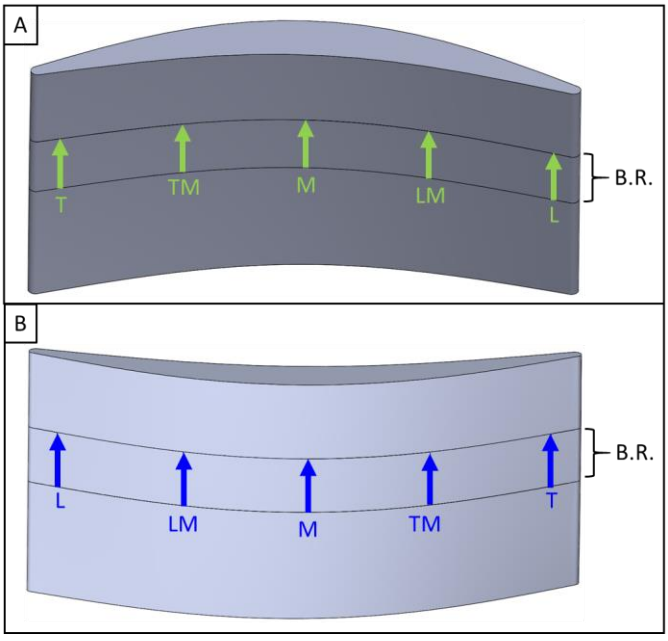

Figure 36 CMM inspection paths for quantifying blendline heights. (A) five probing paths within blendline region (B.R.) on concave side, (B) five probing points on convex side.

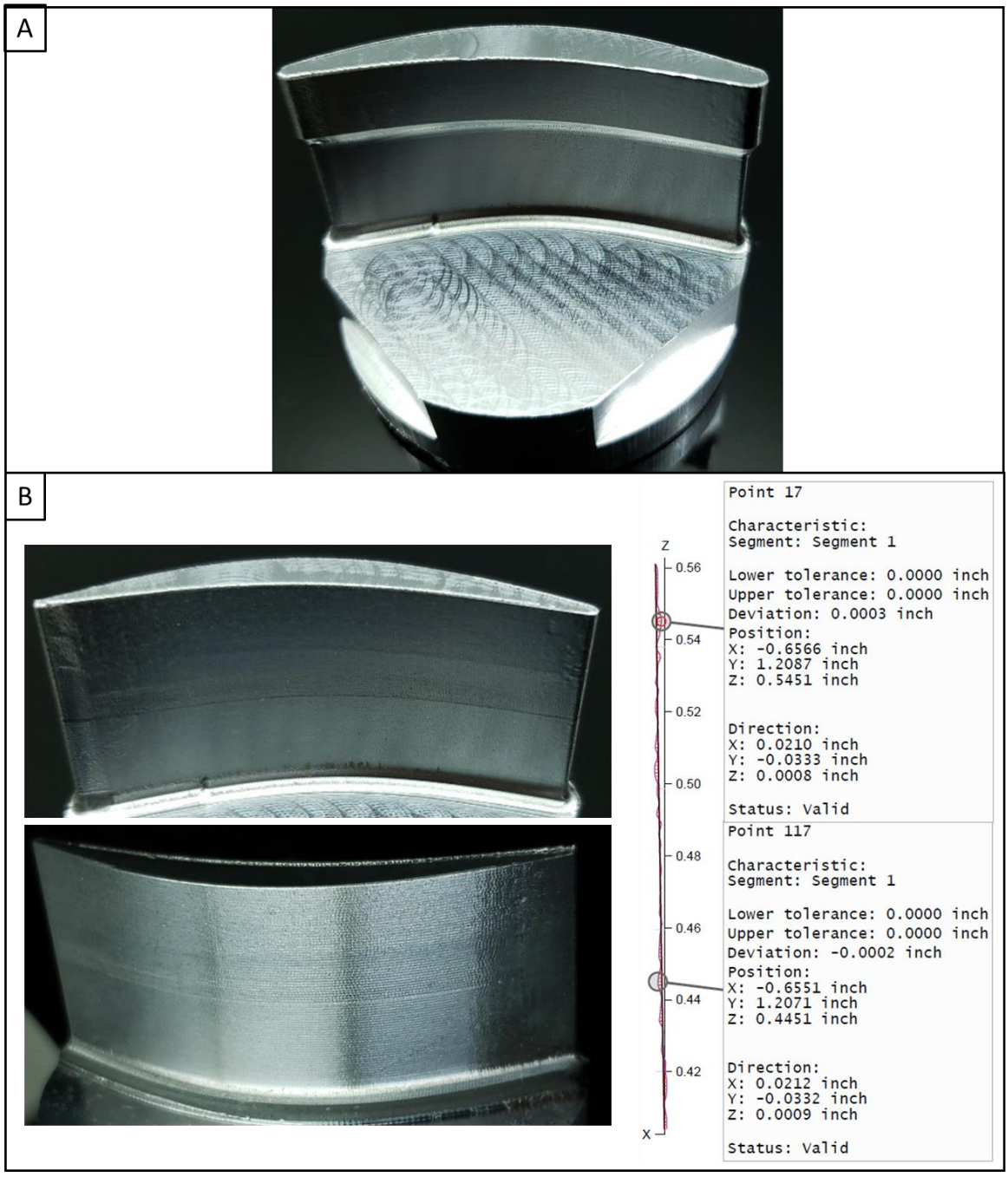

Figure 37 Machined blades and representative blendline height CMM results. (A) machined welded blade. (B) Blade is machined by toolpath created based on the registered geometry using DS digitization method.

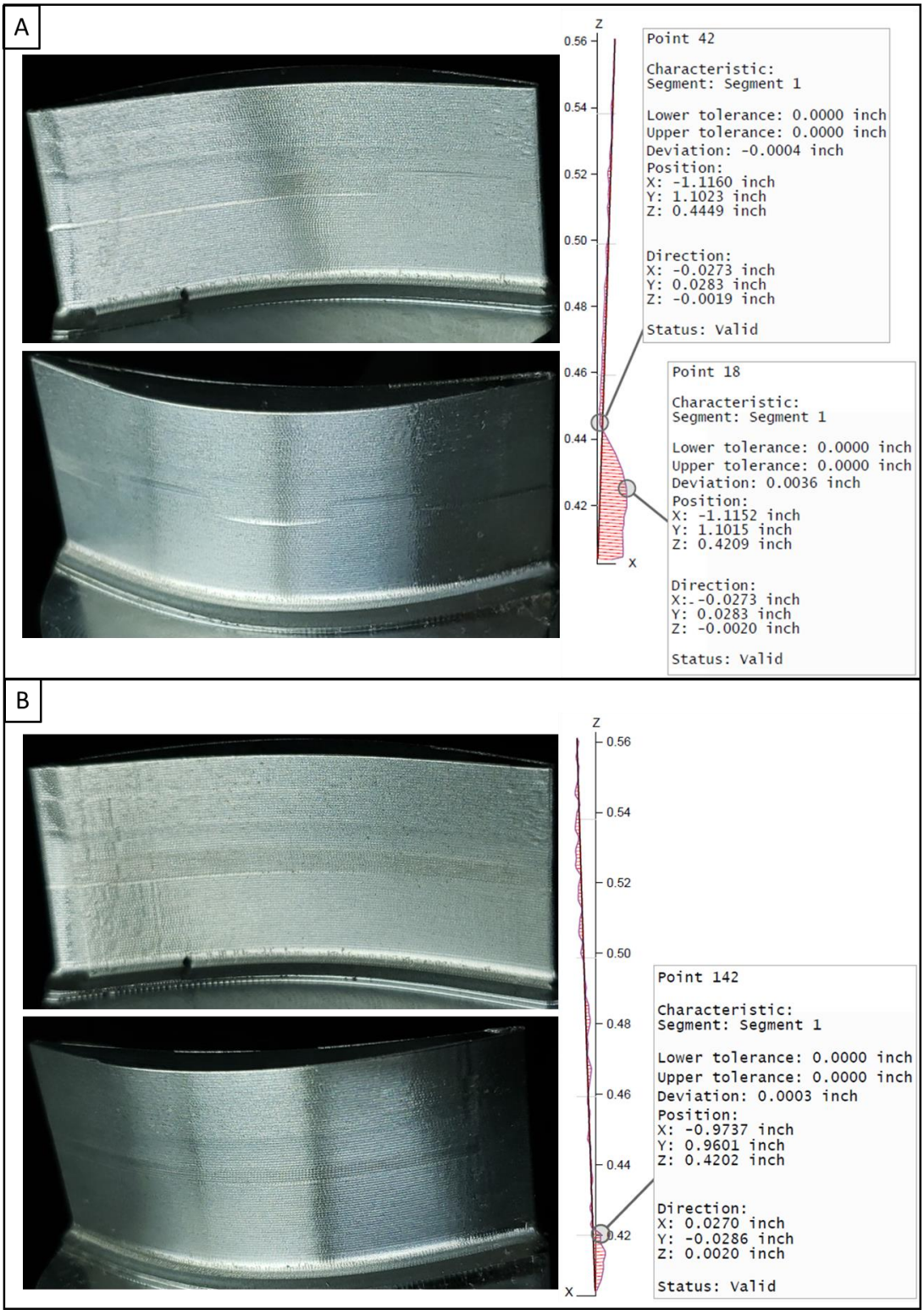

Figure 38 Machined blades and representative blendline height CMM results. Blades are machined by toolpath created based on the registered geometry using following digitization method: (A) G1 continuity method, (B) local maximum control method.

The inspection paths were conducted at five equidistant positions on the concave and convex side to capture effects across the blendline region of the blade geometry. Each position was inspected starting from a height of 0.411 inch to 0.561 inch, drawn as the lower line and the upper line of the blendline region (B.R.) in Figure 36. Zeiss Micura CMM was used for this purpose with a probe stylus ball tip radius of 0.03 inch, scanning speed of 0.05inch per second, and measurement point spacing of 0.001 inch. The Zeiss Micura CMM has a scanning error of 35.4 uin and form measurement error of 31.5 uin.

Machined geometries for the surrogate welded (Figure 37A) and finish blended blades, as well as the CMM inspection results used to determine the blendline step geometry are shown in Figure 34. Of the five digitization methods applied to non-rigid registration, three machined results, which are the DS (Figure 34B), G1 continuity (Figure 34C), and local maximum control method (Figure 34D) are shown with corresponding representative CMM results. Visually, the DS and local maximum control methods (Figure 34B, D) seem to have a blendline due to machining, but when they were measured with a CMM, they only had a blendline step of 0.0003 inch. The periodic characteristic of the simulated deviation observed in the CBS, and G1/G2 continuity methods are also visually observable in the convex side of the blade as shown in Figure 34C.

The CMM results are plotted to better represent the deviation along z axis as in Figure 39A, and the measured maximum blendline height for each method is tabulated and drawn in Figure 39B. The CMM results for the DS and local maximum control methods have the same maximum blendline height of 0.0003 inch. The remaining three methods have almost identical CMM results in all ten parts of the blade with 0.0041 inch being their

maximum blendline height. All measured blendline heights are less than or equal to 0.0002 inch from the simulated surface deviation.

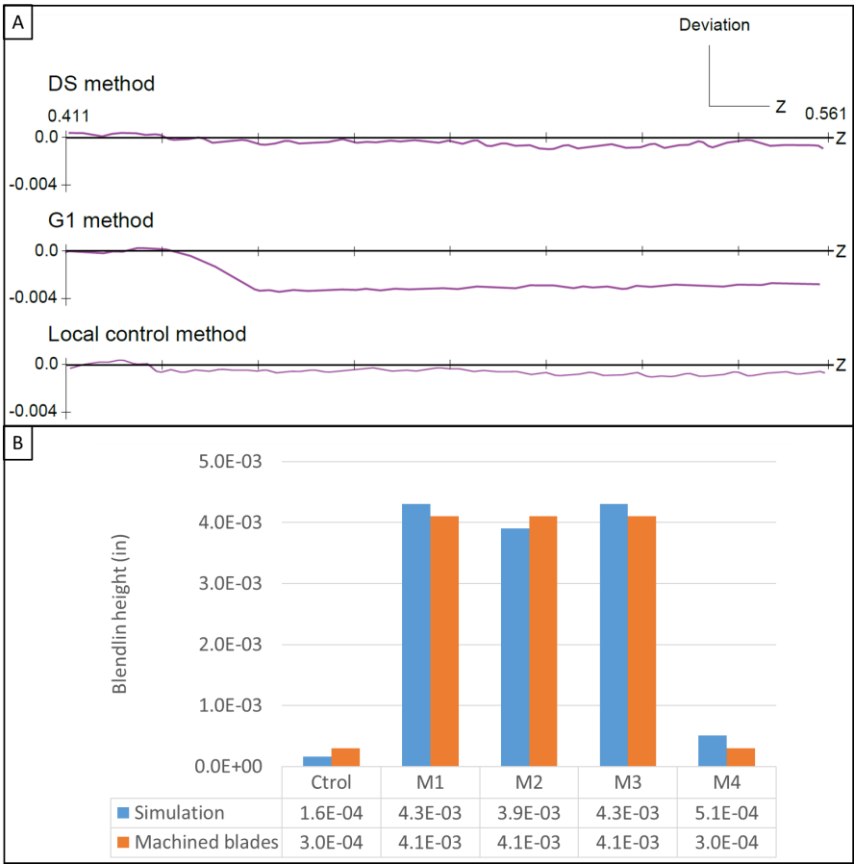

Figure 39 CMM results compared with simulated surface deviation. (A) three representative CMM results showing deviation along z axis, (B) comparison between simulated and measured blendline height.

The deviation analysis and measurements of the simulated and machined blades were investigated further by varying the deformation seen in the used blade through simulation-based study. From the results, the surface deviation observed in the non-rigidly registered blade is due to the 2D profile deviation in the digitization and reconstruction algorithm by comparing the DS method and the remaining four methods. The robustness of the non-rigid registration algorithm is studied using four sample blades with different

values for angular distortion and linear deviation of the chord length as it is tabulated in Table 3[8]. With different parameters in angular distortion (±3º/inch along the stacking axis) and chord length change (±2.28×10^{-3}inch/inch), the results are all within the set tolerance value (0.0005 inch) except for one sample with the maximum surface deviation of 6.1×10^{-4} inch. The maximum values in the table, however, are prone to be found at the tip geometry of the blade which is not the region of interest in this study. Thus, the surface deviation in the blendline region is expected to be lower than the maximum values. Therefore, with the DS and local maximum control digitization method, non-rigidly registering a nominal blade to a deformed blade is most likely to work under these extreme distortion conditions.

Table 3 Surface deviation in sample blades with different distortion parameters [1]

Distortion parameters in blade		Max. surface deviation	Average surface deviation	Standard deviation
Angular (º/inch)	Chord length (inch/inch)			
-3	2.28×10^{-3}	6.1×10^{-4}	2.8uin	62uin
-3	-2.28×10^{-3}	4.9×10^{-4}	1.6uin	78uin
3	-2.28×10^{-3}	2.5×10^{-4}	3.9uin	73uin
3	2.28×10^{-3}	2.6×10^{-4}	2.0uin	60uin

From these results, the model developed to simulate blendline defect geometry based on profile digitization approaches is accurate and can be used to determine optimal digitization approaches that balance quality requirements with time required to probe the part geometry using on-machine probing. In this regard, one can optimize the profile digitization method with more points at appropriate positions to reduce maximum profile

deviation resulting from non-rigid registration. The optimized digitization method can also be used to guide an adaptive additive manufacturing toolpath, as suggested in Ref. [8]. In a non-adaptive additive repair, the deposited material in the blade tip would have to accommodate the range of blade deformation conditions and result in an unnecessarily larger profile thickness, resulting in process inefficiency due to increased deposition time, increased machining time, material waste, and potentially lower tool life. Integration of these additive, subtractive and inspection procedures within an HM-based repair framework will provide for significant capabilities in this regard.

CONCLUSION AND RECOMMENDATIONS

This chapter summarizes the original contributions and main conclusions of this thesis and suggests possible areas for future studies.

1.17 Original contributions

In this study, a digitization and reconstruction method for a non-rigid registration algorithm that could be utilized in an adaptive aerospace blade repair process has been presented. The originality of this research lies in establishing a method that can digitize a blade geometry with an unknown angular distortion and wear deformation, as well as accurately reconstruct the blade profile for a non-rigid registration algorithm. This was validated using the simulated results by comparing with actual machined blades using the proposed method. The successful method in this thesis establishes a balance between the number of probe points considering the manufacturing practicality and the dimensional accuracy of the reconstructed profile. This method can ultimately be implemented to a fully automated repair system in a commercial hybrid manufacturing setting that can repair the blade in one setup utilizing probing, welding, and machining.

1.18 Main conclusions

In this study, a method for digitizing and reconstructing a single 2D blade profile using the least amount of probing points and maximizing the dimensional accuracy of the resulting profile was presented. Four methods of digitizing 2D airfoil blade profiles were developed, and their effect on 3D non-rigid registration was investigated in simulation and on machined parts. Dense sampling method was used as a control of the study to show that

enough probing points can accurately recreate 2D profile and register 3D blade tip geometry. Even with high dimensional accuracy of the registered part, however, the number of the probing points were impractical to implement in the manufacturing setting. Then, curvature-based segmentation, and G1/G2 continuity-based methods have been developed having a range of number of probing points, but dimensional accuracy required of the process was not fully achieved. Finally, the local maximum control-based method is developed and successfully digitized and reconstructed the blade profile within the set tolerance with a practical number of probe points (32 probing points) as well as satisfying dimensional accuracy with deviation of 5.1×10^{-4} inch. This result defines an optimized digitization method for blade profile geometry to be digitized and reconstructed with a set tolerance.

The deviation that was observed in the blade profile digitization was consistent with the non-rigidly registered 3D surface geometry. Blades were machined with the toolpath based the registered models and the simulated results were validated with measurements on the machined parts. The effect of digitization was not detrimental nor beneficial to the registration process, but the deviation that existed in the digitization carried over to the registration algorithm. Furthermore, to encompass various deformation conditions, four extreme deformation limits were proven to work with the registration algorithm, and the digitization method would also most likely perform well under these extreme conditions.

1.19 Future work and recommendation

The digitization method using G1/G2 continuity could be improved by adjusting the points that are added adjacent to the intersecting point between segments. Because of the

nature of cubic spline function, the reconstructed spline contains periodic deviation which brings about more deviation than not applying the method. By positioning the points to be added at different places, it could possibly generate the profile with less points and with less deviation.

A particularly interesting subject for future work is in modifying predetermined probing points. Another digitization/reconstruction method to be investigated is relocating the previously created probing points or adding/removing the probing points in the iteration of reconstructing profile. Local maximum control-based method finds the location of the local maximum deviation and only adds a point to it in each iteration. An increase in the maximum deviation is always observed at a region close to where the point is added. By adjusting the previously positioned probing point(s), it seems to be possible to reduce the maximum deviation in every iteration which could lead to less total probing points.

Another interesting subject for future work is to investigate the accuracy of the implementation of these digitization methods. On-machine probing is likely to produce errors associated with normal approach vectors and probing position acquisition. The errors can be characterized with a range of intentional deformations so to optimize digitization methods. To verify the robustness of the method, the actual acquired probing points can be used in digitization and non-rigid registration algorithm to reconstruct 2D profile and register the nominal blade geometry to analyze the deviation.

REFERENCES

[1] J. B. Jones, P. McNutt, R. Tosi, C. Perry, and D. I. Wimpenny, "Remanufacture of turbine blades by laser cladding, machining and in-process scanning in a single machine," 2012.

[2] J. Aschenbruck, R. Adamczuk, and J. R. Seume, "Recent Progress in Turbine Blade and Compressor Blisk Regeneration," *Procedia CIRP,* vol. 22, pp. 256-262, 2014/01/01/ 2014.

[3] W. Kerr and C. Ryan, "Eco-efficiency gains from remanufacturing: A case study of photocopier remanufacturing at Fuji Xerox Australia," *Journal of cleaner production,* vol. 9, no. 1, pp. 75-81, 2001.

[4] R. Steinhilper, "Recent trends and benefits of remanufacturing: from closed loop businesses to synergetic networks," in *Environmentally Conscious Design and Inverse Manufacturing, 2001. Proceedings EcoDesign 2001: Second International Symposium on,* 2001, pp. 481-488: IEEE.

[5] O. Yilmaz, D. Noble, N. N. Gindy, and J. Gao, "A study of turbomachinery components machining and repairing methodologies," *Aircraft Engineering and Aerospace Technology,* vol. 77, no. 6, pp. 455-466, 2005.

[6] Y. Rong, J. Xu, and Y. Sun, "A surface reconstruction strategy based on deformable template for repairing damaged turbine blades," *Proceedings of the Institution of Mechanical Engineers, Part G: Journal of Aerospace Engineering,* vol. 228, no. 12, pp. 2358-2370, 2014.

[7] J. K. Nagel and F. W. Liou, "Hybrid manufacturing system modeling and development," in *ASME 2012 International Design Engineering Technical Conferences and Computers and Information in Engineering Conference,* 2012, pp. 189-198: American Society of Mechanical Engineers.

[8] M. Praniewicz, T. Kurfess, and C. Saldana, "An Adaptive Geometry Transformation and Repair Method for Hybrid Manufacturing," *Journal of Manufacturing Science and Engineering,* vol. 141, no. 1, pp. 011006-011006-8, 2018.

[9] F. Klocke *et al.,* "Turbomachinery component manufacture by application of electrochemical, electro-physical and photonic processes," *CIRP Annals,* vol. 63, no. 2, pp. 703-726, 2014.

[10] "Rolls-Royce Holdings plc. Annual Report 2012."

[11] D. Joyce, "GE Aviation," in *Barclays Capital Industrial Select Conference*, 2012.

[12] J. Gao, J. Folkes, O. Yilmaz, and N. Gindy, "Investigation of a 3D non-contact measurement based blade repair integration system," *Aircraft Engineering and Aerospace Technology,* vol. 77, no. 1, pp. 34-41, 2005.

[13] N. R. Council, *New materials for next-generation commercial transports*. National Academies Press, 1996.

[14] J. Gao, X. Chen, O. Yilmaz, and N. Gindy, "An integrated adaptive repair solution for complex aerospace components through geometry reconstruction," *The International Journal of Advanced Manufacturing Technology,* vol. 36, no. 11-12, pp. 1170-1179, 2008.

[15] S. Soo, R. Hood, D. Aspinwall, W. Voice, and C. Sage, "Machinability and surface integrity of RR1000 nickel based superalloy," *CIRP Annals-Manufacturing Technology,* vol. 60, no. 1, pp. 89-92, 2011.

[16] M. Burger, L. Koll, E. Werner, and A. Platz, "Electrochemical machining characteristics and resulting surface quality of the nickel-base single-crystalline material LEK94," *Journal of Manufacturing Processes,* vol. 14, no. 1, pp. 62-70, 2012.

[17] A. Ruszaj, J. Gawlik, and S. Skoczypiec, "Electrochemical Machining–Special Equipment and Applications in Aircraft Industry," *Management and Production Engineering Review,* vol. 7, no. 2, pp. 34-41, 2016.

[18] Sibum, H. , Güther, V. , Roidl, O. , Habashi, F. , Uwe Wolf, H. and Siemers, C. (2017). Titanium, Titanium Alloys, and Titanium Compounds. In Ullmann's Encyclopedia of Industrial Chemistry, (Ed.). doi:10.1002/14356007.a27_095.pub2

[19] C.-H. Richter, "Structural design of modern steam turbine blades using ADINA™," *Computers & structures,* vol. 81, no. 8-11, pp. 919-927, 2003.

[20] S. Son, H. Park, and K. H. Lee, "Automated laser scanning system for reverse engineering and inspection," *International Journal of Machine Tools and Manufacture,* vol. 42, no. 8, pp. 889-897, 2002.

[21] J. H. Graham, J. Reinwand, R. G. Coriell, and K. Lytle, "Adaptive machining and weld repair process," ed: Google Patents, 2009.

[22] H. Hazby, I. Woods, M. Casey, R. Numakura, and H. Tamaki, "Effects of Blade Deformation on the Performance of a High Flow Coefficient Mixed Flow Impeller," *Journal of Turbomachinery,* vol. 137, no. 12, pp. 121005-121005-9, 2015.

[23] C. Bremer, "Data Management and Adaptive Machining Technology for Efficient Repair and Manufacture of Turbine Components," in *ASME Turbo Expo 2008:*

Power for Land, Sea, and Air, 2008, pp. 415-422: American Society of Mechanical Engineers.

[24] J. M. Wilson, C. Piya, Y. C. Shin, F. Zhao, and K. Ramani, "Remanufacturing of turbine blades by laser direct deposition with its energy and environmental impact analysis," *Journal of Cleaner Production*, vol. 80, pp. 170-178, 2014.

[25] A. L. Mendham, "Method of making replacement airfoil components," ed: Google Patents, 1993.

[26] J. Clark, "Implementing non-contact digitisation techniques within the mechanical design process," *Sensor Review*, vol. 20, no. 3, pp. 195-202, 2000.

[27] J. A. Vargas, J. E. Wilches, H. A. Gómez, J. A. Pacheco, and R. J. Hernandez, "Analysis of catastrophic failure of axial fan blades exposed to high relative humidity and saline environment," *Engineering Failure Analysis*, vol. 54, pp. 74-89, 2015.

[28] Zeiss. (2018, 11/3/2018). *Zeiss T-SCAN 20.* Available: https://www.zeiss.com /metrology/products/systems/optical-systems/3d-scanning/zeiss-t-scan.html

[29] Zeiss. (2018, 11/3/2018). *COMET Pro AE-automated measurement solution.* Available: https://optotechnik.zeiss.com/en/products/3d-scanning/comet-pro-ae

[30] Y. Zhang, D. Zhang, and B. Wu, "A geometry reconstruction approach based on cross-section curve blending for adaptive repair of blades," in 5th International Conference on Responsive Manufacturing - Green Manufacturing (ICRM 2010), 2010, pp. 146-151.

[31] Bremer, C. (2000), “Adaptive strategies for manufacturing and repair of blades and bliks”, paper presented at the 45th ASME International Gas Turbine and Aeroengine Technical Congress, Rottger, Munich, 8-11 May 2000.

[32] Dix B. Aerofoil machining and polishing combined into a single automated process. Aircraft Engineering and Aerospace Technology. 2004; 76(5).

[33] Z. Gong, X. Chen, and H. Huang, "Optimal profile generation in distorted surface finishing," in *Robotics and Automation, 2000. Proceedings. ICRA'00. IEEE International Conference on*, 2000, vol. 2, pp. 1557-1562: IEEE.

[34] H. Huang, Z. Gong, X. Chen, and L. Zhou, "Robotic grinding and polishing for turbine-vane overhaul," *Journal of materials processing technology*, vol. 127, no. 2, pp. 140-145, 2002.

[35] L. Ferrando, J.-L. Kueny, F. Avellan, C. Pedretti, and L. Tomas, "Surface parameterization of a Francis runner turbine for optimum design," in *22nd IAHR Symposium on hydraulic machinery and systems*, 2004.

[36] G. N. Koini, S. S. Sarakinos, and I. K. Nikolos, "A software tool for parametric design of turbomachinery blades," *Advances in Engineering Software*, vol. 40, no. 1, pp. 41-51, 2009.

[37] J. Ashburner and K. J. Friston, "Rigid body registration," *Statistical parametric mapping: The analysis of functional brain images*, pp. 49-62, 2007.

[38] P. Munford, "Autodesk Inventor surfacing. Curvature continuity and sketch constraints," 2014.